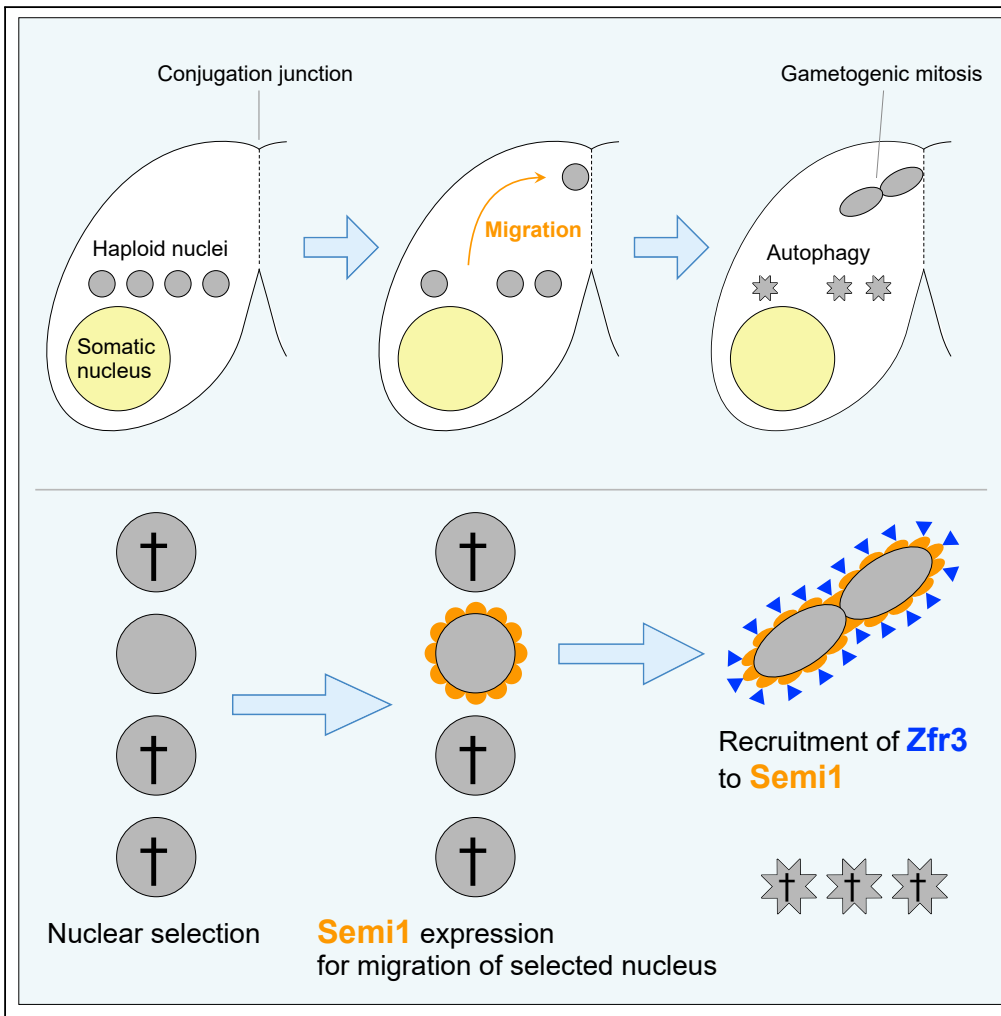


Article

The Transmembrane Protein Semi1 Positions Gamete Nuclei for Reciprocal Fertilization in *Tetrahymena*



Takahiko Akematsu, Rosalía Sánchez-Fernández, Felix Kosta, Elisabeth Holzer, Josef Loidl

ta2576@cumc.columbia.edu

HIGHLIGHTS

The transmembrane protein Semi1 is specifically expressed in mating *Tetrahymena*

Semi1 marks the one nucleus out of four meiotic products that gives rise to pronuclei

Semi1 mediates the attachment of the selected nucleus to the conjugation junction

Semi1 interacts with Zfr3, which mediates the reciprocal exchange of pronuclei

Akematsu et al., iScience 23, 100749
 January 24, 2020 © 2019 The Author(s).
<https://doi.org/10.1016/j.isci.2019.100749>



Article

The Transmembrane Protein Semi1 Positions Gamete Nuclei for Reciprocal Fertilization in *Tetrahymena*

Takahiko Akematsu,^{1,2,3,*} Rosalía Sánchez-Fernández,¹ Felix Kosta,¹ Elisabeth Holzer,¹ and Josef Loidl¹**SUMMARY**

During sexual reproduction in the ciliate, *Tetrahymena thermophila*, cells of complementary mating type pair (“conjugate”) undergo simultaneous meiosis and fertilize each other. In both mating partners only one of the four meiotic products is “selected” to escape autophagy, and this nucleus divides mitotically to produce two pronuclei. The migrating pronucleus of one cell translocates to the mating partner and fuses with its stationary pronucleus and vice versa. Selection of the designated gametic nucleus was thought to depend on its position within the cell because it always attaches to the junction with the partner cell. Here we show that a transmembrane protein, Semi1, is crucial for attachment. Loss of Semi1 causes failure to attach and consequent infertility. However, a nucleus is selected and gives rise to pronuclei regardless of Semi1 expression, indicating that attachment of a nucleus to the junction is not a precondition for selection but follows the selection process.

INTRODUCTION

The model ciliate *Tetrahymena thermophila* stably maintains different germline and somatic genomes in two separate nuclei within a single cytoplasm. The small diploid micronucleus (MIC), which is essentially transcriptionally silent, contains the germline genome, whereas the large, transcriptionally active polyploid macronucleus (MAC) contains the somatic genome. The phenotype of a cell depends on the genetic constitution of its MAC, whereas only the MIC genome is transmitted to progeny MICs and MACs during sexual reproduction (Figure 1A, left panel), also known as conjugation (Prescott, 1994; Orias et al., 2011). When two cells of complementing sexes (mating types) conjugate, they undergo synchronous meiosis. Meiosis of the MIC produces four identical haploid MICs (hMICs) that are in the G2 phase of the cell cycle due to DNA replication, which takes place concomitantly with meiotic anaphase II (Cole and Sugai, 2012). After meiosis, only one hMIC is selected to form the gamete, whereas the three unselected hMICs are degraded by autophagy (Liu and Yao, 2012). All four meiotic products undergo post-meiotic DNA double-strand break (PM-DSB) formation. DNA damage in hMICs correlates with the appearance of γ H2AX foci (Akematsu et al., 2017), which are markers of DSBs (Chowdhury et al., 2005; Kadoch and Crabtree, 2015). The γ H2AX foci disappear only from one hMIC, and this occurs at the same time as histone H3 becomes acetylated at lysine 56 (H3K56ac), which is an epigenetic marker of reconstituted chromatin on nascent DNA (Shi and Oberdoerffer, 2012; Chen et al., 2008). Only this hMIC undergoes another round of mitosis, known as gametogenic mitosis, to produce gametic pronuclei (Akematsu et al., 2017). One of the pronuclei migrates to the partner cell to fertilize its stationary pronucleus, whereas the other becomes fertilized by the migratory pronucleus of the partner cell. This reciprocal fertilization leads to the formation of zygotes in both partners. Attenuated PM-DSB formation culminates in autophagy for all hMICs (Akematsu et al., 2017), strongly suggesting that hMIC selection involves self-inflicted DNA damage in all hMICs followed by DNA repair in only one. Indeed, the DNA repair proteins DNAPKcs (involved in DNA repair by non-homologous end-joining) and Rad51 (involved in recombinational repair) and the histone H3-H4 chaperone Asf1 specifically localize to the selected hMIC (Akematsu et al., 2017).

In the related species, *Paramecium caudatum*, the fate of hMICs is proposed to depend on their position in the cell (Yanagi, 1987). In this species, an hMIC that happens to be in contact with the conjugation junction (where the plasma membranes of conjugating cells are fused) may be protected from autophagic degradation by its location in this specific microenvironment and thus able to recruit DNA repair proteins. Indeed in both *P. caudatum* (Ishida et al., 1999; Gao et al., 2010) and *T. thermophila* (Cole and Sugai, 2012), the hMIC located at the junction is always selected to undergo gametogenic mitosis. However, two fundamental questions remain: (1) how does the hMIC attach to the conjugation junction (hereafter called

¹Department of Chromosome Biology, University of Vienna, Dr. Bohr-Gasse 9, Vienna 1030, Austria

²Present address: Department of Biochemistry and Molecular Biophysics, Columbia University, 701 West 168 Street, New York, NY 10032, USA

³Lead Contact

*Correspondence: ta2576@cumc.columbia.edu
<https://doi.org/10.1016/j.isci.2019.100749>



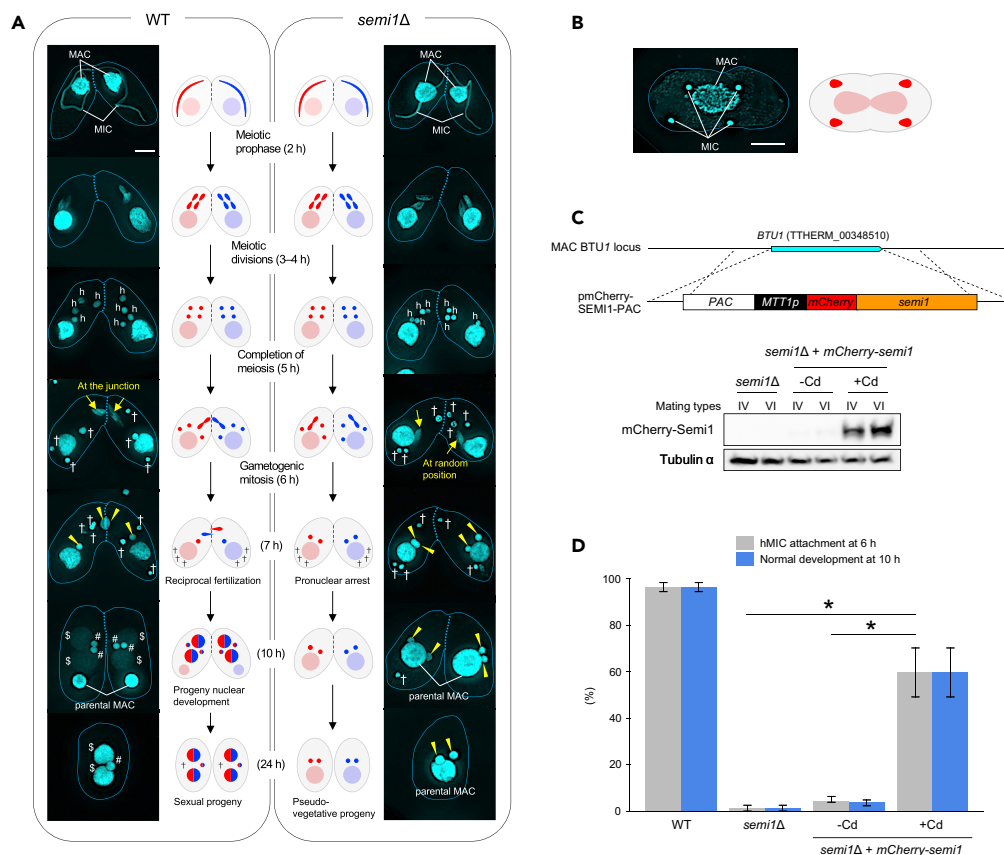


Figure 1. Semi1 Mediates hMIC Attachment to the Conjugation Junction

(A) Timeline of conjugation in WT (left) and *semi1* Δ (right) cells (see also Figures S1C and S1D) stained with DAPI, shown as fluorescence microscopy images and schematic diagrams. h: hMICs; arrows: selected hMICs undergoing gametogenic mitosis; \dagger : degenerating unselected hMICs; \rightarrow : gametic pronucleus; $\$$: progeny MACs; #: progeny MIC. Dotted line: conjugation junction.

(B) Image (left) and diagram (right) of vegetative division of a *semi1* Δ exconjugant, in which unexchanged gametic pronuclei are maintained (see also Figure S1E). Scale bar: 10 μ m.

(C) Rescue of the *semi1* Δ phenotype by *semi1*-mCherry expression. The pmCherry-SEMI1-PAC plasmid, containing a puromycin resistance marker (PAC), cadmium-inducible MTT1 promoter, and mCherry-Semi1-expression cassette, was integrated into the MAC *BTU1* locus by homologous recombination. The Western blot shows that mCherry-Semi1 expression is induced by the addition of cadmium. Tubulin α was the loading control.

(D) Percentage of cells with normal hMIC attachment at 6 h after the initiation of conjugation (see also Figure S2) and development of progeny nuclei at 10 h. Columns and error bars represent the means and standard deviations of three independent experiments. Asterisk (*) shows a significant difference between means ($p < 0.01$ as calculated by Tukey's honestly significant difference [HSD] test on RStudio).

“hMIC attachment”) and (2) is hMIC attachment a key molecular switch that controls hMIC selection? Here, we report that the protein Semi1 (selected haploid micronucleus 1) is key to understanding the mechanism of hMIC attachment and the behavior of the selected nucleus.

RESULTS

Semi1 Mediates hMIC Attachment to the Conjugation Junction

Semi1 (711 aa, 84 kDa, encoded by TTHERM_00985030; www.ciliate.org) is a putative transmembrane protein in *T. thermophila* (Figure S1A) that has no known homolog in other organisms. A genetic screen for genes that are transcriptionally upregulated during the pre-zygotic period of conjugation (Miao et al., 2009) found that *SEMI1* is required for conjugation, and western blotting demonstrated that Semi1 protein is expressed only in conjugating cells (Figure S1B). Somatic knockout (*semi1* Δ) cells of two different sexes (mating types) were produced by co-deletion (co-Del), which uses the natural DNA elimination mechanism

of *T. thermophila* to target specific sequences with flanking deletion signal motifs (Figures S1C and S1D) (Hayashi and Mochizuki, 2015). DAPI (4',6-diamidino-2-phenylindole) nuclear staining showed that *semi1Δ* mating cells undergo meiosis and produce four hMICs at 5 h after the initiation of conjugation, similar to wild-type (WT) mating cells (Figure 1A). However, most *semi1Δ* mating cells initiated gametogenic mitosis in an hMIC that was not attached to the conjugation junction at the 6 h time point (Figure 1A). No pronuclei exchange occurred between the mating partners (Figure 1A), and the single hMIC undergoing mitosis in each cell was retained, whereas the unselected hMICs had disappeared by 10 h (Figure 1A). Mating in *semi1Δ* was completed by 24 h, with each progeny cell containing two MICs and the parental MAC (i.e. pseudo-vegetative progeny; Figure 1A). The two MICs were maintained during asexual division of the ex-conjugants (Figures 1B and S1E). Unlike in the similar process of autogamy in *Paramecium tetraurelia* (Garnier et al., 2004; Komori et al., 2004), self-fertilization did not occur.

Because co-Del can create off-target changes in the genome (Hayashi and Mochizuki, 2015), it was formally possible that the aberrant conjugation phenotype in *semi1Δ* cells could have resulted from off-target mutations. In fact, an analysis showed that about 700 bp extra non-coding sequences were deleted together with the target sequence in both sexes (Figure S1C). To show that deletion of the target gene was responsible for the aberrant conjugation phenotype, an mCherry-tagged Semi1 (mCherry-Semi1) construct expressed under the cadmium-inducible *MTT1* promoter (Shang et al., 2002) was introduced into the non-essential β -*tubulin* genomic locus of *semi1Δ* cells (Figure 1C). Induction of mCherry-Semi1 expression (Figure 1C) partially rescued the phenotype: over 60% of *semi1Δ* + *mCherry-semi1* cells underwent gametogenic mitosis at the conjugation junction and formed progeny nuclei (Figure 1D). Therefore, the aberrant conjugation phenotype in *semi1Δ* is unlikely to result from the off-target effects of co-Del.

The mCherry-Semi1 construct (Figure 1C) was introduced to WT cells for the localization of Semi1. mCherry-Semi1 localized to a single hMIC (Figure 2A). This was the only nucleus to attach to the conjugation junction, followed by gametogenic mitosis, gametic pronuclear exchange, and karyogamy (Figure 2A), which is characteristic of the selected hMIC. Because mCherry-Semi1 expression in the selected hMIC overlaps with the expression pattern of GFP-tagged Nup93 (GFP-Nup93; Figure 2B) (Iwamoto et al., 2009), Semi1 is likely to be a nuclear membrane protein. Mutagenesis analysis showed that all four hydrophobic regions of Semi1, including the transmembrane helix, were required for its perinuclear localization (Figures S2A–S2E). Moreover, none of the mutant Semi1 proteins could rescue the *semi1Δ* phenotype in co-expression experiments (Figure S2F). We therefore suggest that perinuclear localization of Semi1 is required for regulation of hMIC attachment to the conjugation junction.

DNA Repair Markers Indicate that hMIC Selection Occurs without hMIC Attachment in *semi1Δ* Cells

In *P. caudatum*, selection of an hMIC is proposed to involve its attachment to the conjugation junction (Yanagi, 1987). If this were also the case in *T. thermophila*, then none of the hMICs in *semi1Δ* cells would undergo DNA repair and they all would be degraded. Remarkably, however, one hMIC undergoes mitosis in the *semi1Δ* mutant irrespective of its position within the cell (Figures 1A and 3A). To explore whether this nucleus bears the γ H2AX and H3K56ac marks upon repair of PM-DSBs that are characteristic of a selected hMIC (Akematsu et al., 2017), double immunostaining of γ H2AX and H3K56ac was performed in *semi1Δ* cells.

We observed γ H2AX foci in all four hMICs in *semi1Δ* cells at 4.5 h after the initiation of conjugation, as seen in WT cells (Figure 3A), indicating that PM-DSB formation is independent of Semi1 expression. In contrast, only the MAC displayed H3K56 acetylation, which is consistent with its euchromatic state at this time point (Figure 3A). After 6 h, only one hMIC had initiated gametogenic mitosis in *semi1Δ* cells, and in this hMIC H3K56 acetylation occurred concomitantly with the disappearance of γ H2AX (Figure 3A). This result strongly suggests that hMIC attachment to the conjugation junction is not required for DNA repair. Analysis of EGFP-DNAPKcs and Rad51 localization showed that these major DNA repair factors were recruited only to the hMIC undergoing gametogenic mitosis, regardless of Semi1 expression (Figures 3B and 3C).

To test whether positional cues other than association with the conjugation junction may determine the fate of hMICs, we marked the selected hMIC with EGFP-DNAPKcs in *semi1Δ* cells (Figure 3D) and determined its position within the cells. We found that the selected hMIC preferentially resides in the space between the MAC and the conjugation junction (Figure 3E), whereas the unselected hMICs are more evenly

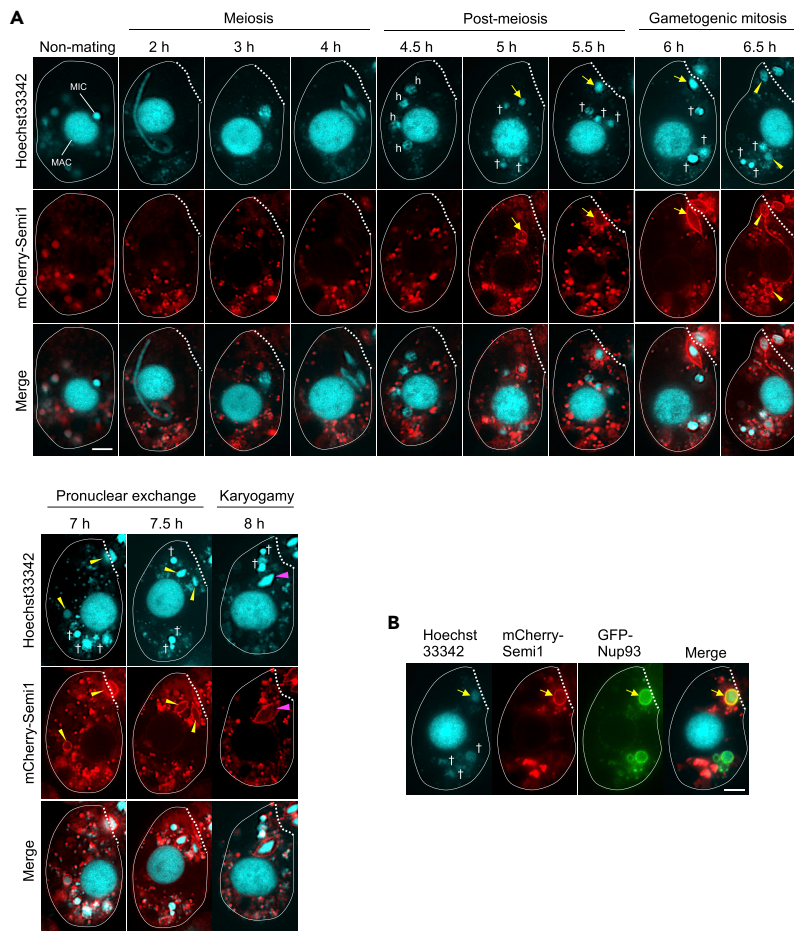


Figure 2. Live Cell Imaging of mCherry-Semi1 Localization

(A) mCherry-Semi1 is localized to the hMIC selected for gametogenic mitosis. The bright spheres in the cytoplasm are digestive vacuoles probably incorporating overexpressed or unfolded mCherry-Semi1.

(B) mCherry-Semi1 and GFP-Nup3 co-localize at the periphery of the selected hMIC in live cells. h: hMIC; arrow: selected hMIC undergoing gametogenic mitosis; †: degenerating unselected hMIC; yellow arrowheads: gametic pronucleus; magenta arrowhead: fertilized nucleus; dotted line: conjugation junction. Scale bars: 10 μ m.

distributed throughout the cell (Figure 3F) at the time when they begin to move toward the posterior part, which is highly enriched in lysosomes (Akematsu et al., 2017). Thus, although hMIC selection does not take place in the vicinity of the conjugation junction, its location may not be completely random.

Semi1 Acts on the MAC in the Absence of hMIC Selection

Given that mCherry-Semi1 localizes exclusively to the selected hMIC (Figure 2A), it is possible that Semi1 may have an affinity for molecules that appear on its nuclear envelope upon hMIC selection. If so, mCherry-Semi1 should not be expressed in the hMIC of mutants in which hMIC selection does not occur. To confirm this, we expressed mCherry-Semi1 in *spo11 Δ* cells, where hMIC selection is prevented by PM-DSB suppression (Akematsu et al., 2017).

As predicted, mCherry-Semi1 did not localize to any hMIC in *spo11 Δ* cells at 6 h after the initiation of conjugation (Figure 4A), when all hMICs are programmed to degenerate. Notably, a clear mCherry-Semi1 signal became apparent at the periphery of the MAC after 7 h in *spo11 Δ* cells (Figure 4A) but not in the WT (Figure 2A). Remarkably, the MAC in the *spo11 Δ* cells (i.e. with the mCherry-Semi1 signal) became somewhat elongated and was attached to the conjugation junction at 12 h (Figure 4A). This phenomenon resembles the aberrant MAC elongation toward the conjugation junction seen in the inbred mutant strain B1, in which

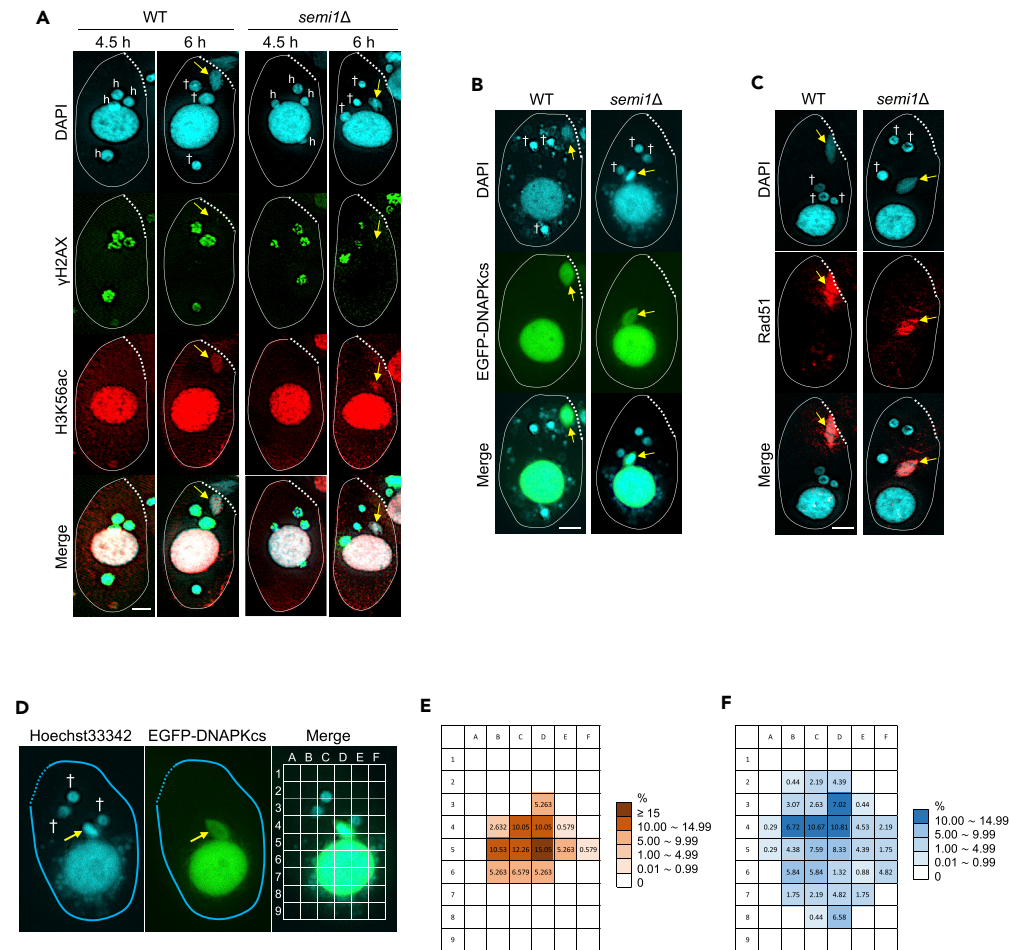


Figure 3. DNA Repair Markers Indicate that hMIC Selection Occurs without hMIC Attachment in *semi1Δ* Cells

(A) γ H2AX foci are formed in all four hMICs of both WT and *semi1Δ* cells but are lost in only one hMIC (arrow), concomitant with histone H3 acetylation at lysine 56 (H3K56ac).

(B) Localization of EGFP-DNAPKcs in a single hMIC (arrow) in both WT and *semi1Δ* cells at 6 h after the initiation of conjugation.

(C) Localization of Rad51 in an hMIC (arrow).

(D) The position of the selected hMIC (arrow) and unselected hMICs (†) in *semi1Δ* cells expressing EGFP-DNAPKcs was determined using a 9 × 6 grid.

(E) Heatmap showing the cytoplasmic distribution of selected hMICs.

(F) Heatmap showing the cytoplasmic distribution of unselected hMIC. The heatmaps were based on data from 17 cells with a clearly defined selected MIC and 17 cells with four unselected MICs. h: hMIC; dotted line: conjugation junction; arrow: selected hMICs undergoing gametogenic mitosis; †: degenerating unselected hMIC. Scale bars: 10 μ m.

hMIC selection is defective (Nanney and Nagel, 1964). About 60% of *spo11Δ* cells showed the MAC attachment phenotype (Figures 4B and 4C). To determine whether MAC attachment to the conjugation junction is Semi1 dependent, a cadmium-inducible *semi1* RNA interference (RNAi) construct (*semi1i*; Figure S3) was introduced into *spo11Δ* cells. *semi1i* expression significantly reduced the proportion of cells with MAC attachment (from 60% to 12%; Figure 4C), strongly suggesting that Semi1 attaches the MAC to the conjugation junction instead of the selected hMIC when hMIC selection is lacking.

Proteomic Analysis of Semi1

Considering its localization and role in attachment to the conjugation junction, Semi1 may mediate the attachment between surface proteins on both the selected hMIC and the conjugation junction. To investigate this possibility, interaction partners of mCherry-Semi1 were co-immunoprecipitated and identified by mass spectrometry (MS). Cells expressing the free mCherry tag (Figure S2A) were used as

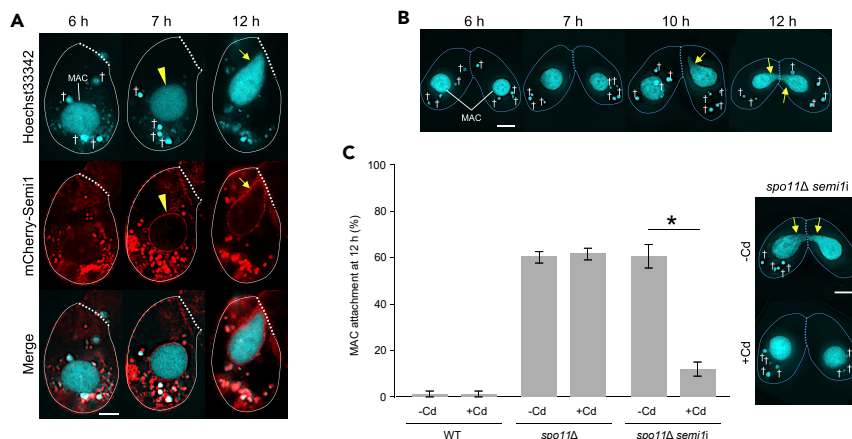


Figure 4. Semi1 Acts on the MAC in the Absence of hMIC Selection

(A) Localization of Semi1 in a *spo11Δ* strain, which is defective in hMIC selection. †: degenerating unselected hMIC; arrowhead: MAC bearing mCherry-Semi1; arrows: MAC elongating toward the conjugation junction.

(B) In *spo11Δ* cells, MAC attachment to the conjugation junction occurs between 6 h and 12 h after the initiation of conjugation.

(C) Left, percentage of cells showing MAC attachment at 12 h after the initiation of conjugation. Columns and error bars represent the means and standard deviations of three independent experiments. Asterisk (*) shows a significant difference ($p < 0.01$, as calculated by Tukey's HSD test on RStudio). Right, examples of conjugating *spo11Δ semi1i* (uninduced) and *spo11Δ semi1i* (induced) cells (see also Figure S3). Arrow: selected hMIC undergoing gametogenic mitosis; †: degenerating unselected hMIC; arrowhead: gametic pronucleus; dotted line: conjugation junction. Scale bars: 10 μ m.

the control. SAINTexpress analysis (Teo et al., 2014) of the MS data revealed 65 potential interaction partners ($p < 0.05$) of which 12 appeared to have conjugation-specific expression (Tables 1 and S1). Of these, Zfr3 (Zinc Finger-Related 3; encoded by THERM_00531890) was the most abundant (see below). Another constitutively expressed Semi1 interactor was 14-3-3 protein 18 (Ftt18; Table S1). Interestingly, enhanced green fluorescent protein (EGFP)-tagged Ftt18 (Ftt18-EGFP) localized to both the conjugation junction and the periphery of the selected hMIC (Figure S4), suggesting that a strong binding affinity between Semi1 and Ftt18 may generate the cohesive force behind hMIC attachment to the conjugation junction. Indeed, 14-3-3 proteins are known to bind a multitude of functionally diverse proteins, including transmembrane proteins (Fu et al., 2000). Unfortunately, the function of Ftt18 is unknown and was difficult to determine because the *FTT18* gene seems to be essential for vegetative growth. In addition, a specific RNAi construct for *FTT18* was difficult to design because of high sequence similarity between *FTT18* and the other two *FTT* paralogs (THERM_00592720 and THERM_00160770).

Zfr3-mediated Gametic Pronuclear Exchange Is Dependent on Semi1

The gene encoding Zfr3 is also called *Coi9* (conjugation-induced gene 9) because of its conjugation-specific expression (Woehrer et al., 2015). The Zfr3 protein contains a zinc finger structure (Figure S5A) but has no clear homologs in other organisms. A previous knockout study reported that macronuclear *ZFR3* is required for proper conjugation (Xu et al., 2012; Woehrer et al., 2015). However, the timing and mechanism of its role in conjugation was unclear. To further investigate the function of Zfr3 and its relation to Semi1, we drastically reduced Zfr3 expression using *zfr3* RNAi (*zfr3i*; Figure S5B).

In the non-induced state, *zfr3i* mating cells underwent conjugation normally and completed the process as exconjugants (Figure 5A). In contrast, in the induced state, most *zfr3i* cells were di-micronuclear single cells and retained the parental MAC (Figures 5A and 5B), similar to the *semi1Δ* mutant (Figure 1A). Further, four hMICs were formed (Figure 5A), showing that meiosis was normal. Moreover, the markers of DNA repair (i.e. the disappearance of γ H2AX foci and concomitant H3K56 acetylation and DNAPKcs and Rad51 localization) were seen in only one of the hMICs (Figures S5C–S5E), indicating that Zfr3 is not involved in hMIC selection. However, unlike in *semi1Δ* cells, gametogenic mitosis occurred in close proximity to the conjugation junction at 6 h after the initiation of conjugation (Figure 5A). Indeed, visualization of the nuclear rim with mCherry-tagged Nup93 (mCherry-Nup93; Figure S5G) clearly showed the selected

Gene ID (THERM_)	AvgCount	Control Count	P Value	Protein Name	Description
00985030	383	2 33	0	Semi1	Transmembrane protein putative
00531890	45	0 9	0.01	Zfr3	Zinc finger domain containing protein
000158019	22.5	0 1	0	None	Hypothetical protein
00083300	17	0 1	0	None	Cullin family protein
00442210	16	0 6	0.02	Rpn2	RPN1 26S proteasome regulatory complex subunit RPN2
00703970	13.5	0 0	0	Ima5	IMA5 import in subunit alpha putative
00437600	10	0 1	0	None	Succinyl-CoA ligase [GDP-forming] subunit beta
01079260	9.5	0 0	0	None	ATP-dependent metalloprotease FtsH
00221140	9	0 0	0	Ars2	ARS2 alanine-tRNA ligase/alanyl-tRNA synthetase protein
00624630	9	0 3	0.01	None	Transmembrane protein putative
00158020	6	1 1	0.02	None	PCI-domain protein
00444470	5.5	0 1	0	None	S-adenosylmethionine synthase protein
00294640	5	2 1	0.05	None	NADH-ubiquinone oxidoreductase 1 chain putative

Table 1. MS Identification of Conjugation-specific Interaction Partners with Semi1

See also Table S1 and Figure S4.

hMIC attached to the conjugation junction in *zfr3i* cells (Figure 5C). These results suggest that loss of Zfr3 may affect either the exchange or the karyogamy of gametic pronuclei. To address this question, we labeled the MIC in cells of one mating type with 5-ethynyl-2'-deoxyuridine (EdU) prior to conjugation (Figure 5D). In the WT control, EdU was present in progeny MACs and MICs of both mating cells at 10 h due to pronuclear exchange followed by karyogamy (Figure 5D). In contrast, in *zfr3i* mating cells, EdU-incorporated DNA remained in the gametic pronuclei of cells of the original mating type (Figure 5D). We therefore conclude that Zfr3 is required for gametic pronuclear exchange (Figure 5E). As expected, pronuclear exchange did not take place in *semi1Δ* mating cells (Figure 5D).

To analyze the subcellular localization of Zfr3, a strain expressing EGFP-tagged protein (EGFP-Zfr3) was created (Figure S5F) and mated with a strain expressing mCherry-Semi1. We found that EGFP-Zfr3 began to localize to the periphery of the selected hMIC simultaneously with mCherry-Semi1 (Figure 5F), whereas in *spo11Δ* mating cells, both fusion proteins co-localized at the periphery of the elongating MAC (Figure 5G). During pronuclear exchange, EGFP-Zfr3 strongly accumulated at the conjugation junction (Figure 5F), reflecting the likely role of Zfr3 in the exchange process. In the absence of Semi1 (by *semi1i* expression or in the *spo11Δ* background), EGFP-Zfr3 localized to neither the selected hMIC or MAC nor the conjugation junction, but instead formed numerous fibrous structures near to the conjugation junction (Figures 5H and 5I). In contrast, in the absence of Zfr3, mCherry-Semi1 localized normally to the selected hMIC in the WT background (Figure 5J) and to MAC in the *spo11Δ* background (Figure 5K). These results indicate that Semi1 is critical for both the correct localization and function of Zfr3. The fact that Zfr3 formed fibrous structures in the absence of Semi1 (Figures 5H and 5I) suggests that Zfr3 may be able to bind to the protein meshwork formed around the conjugation junction (Numata et al., 1985; Orias et al., 1983; Takagi et al., 1991) to promote gametic pronuclear exchange. Overall, these results show that Semi1 is essential for recruiting the selected hMIC to the conjugation junction to enable gametic pronuclear exchange (Figure 6).

DISCUSSION

hMIC Selection Is Independent of Attachment to the Conjugation Junction

Different ciliate species contain differing numbers of MICs (from one to ~20) and, hence, differing numbers of hMICs (from four to ~80) following meiosis (Prescott, 1994). However, regardless of the number of hMICs formed, only one becomes the gametic pronucleus (Prescott, 1994). In addition, only one hMIC is selected

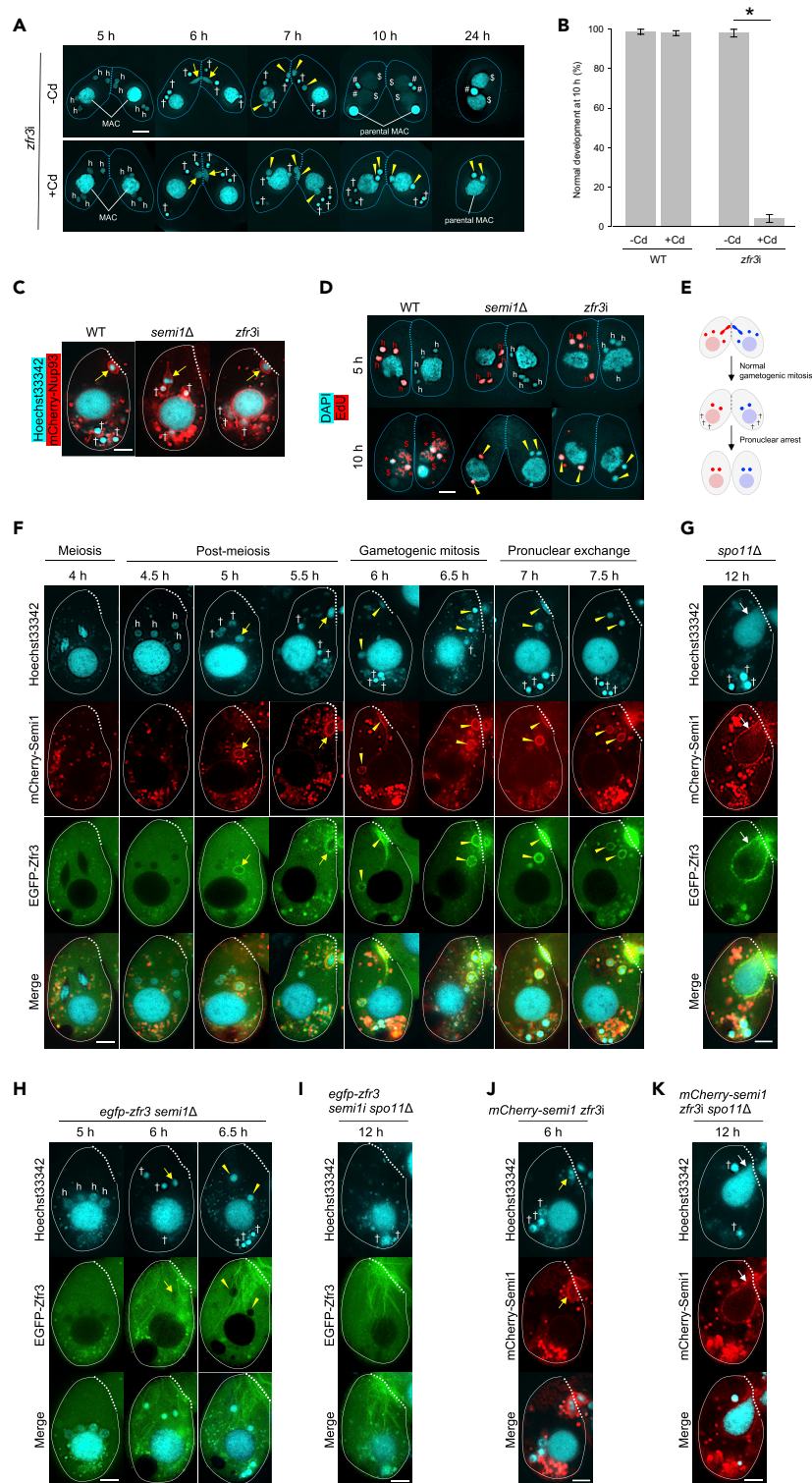


Figure 5. Zfr3-mediated Gametic Pronuclear Exchange Is Dependent on SEMI1

(A) Conjugating *zfr3i* cells (see also Figure S5) stained with DAPI. Top row, uninduced cells; bottom row, *zfr3i* RNAi induced by CdCl₂.

Figure 5. Continued

(B) Percentage of cells with normal development of progeny nuclei at 10 h after the initiation of conjugation. Columns and error bars represent the means and standard deviations of three independent experiments. Asterisk (*) shows a significant difference ($p < 0.01$, as calculated by Tukey's HSD test on RStudio).

(C) *zfr3i* does not affect hMIC attachment to the conjugation junction. The rim of the selected hMIC was visualized by mCherry-Nup93.

(D) EdU (red) was incorporated into the MIC (left cell) for monitoring MIC exchange. hMICs remain in the labeled cell at 5 h after the induction of meiosis. EdU labeling is seen in both cells at 10 h in the WT and is restricted to the labeled cell in the *semi1Δ* and *zfr3i* genotypes.

(E and F) (E) Pronuclear arrest phenotype of *zfr3i* cells. Different colors in the nuclei denote different genetic compositions as shown in Figure 1A. (F) Localization of Zfr3 in WT cells.

(G) Localization of Zfr3 in *spo11Δ* cells. White arrow: MAC elongating toward the conjugation junction.

(H) Zfr3 does not localize to the selected hMIC in *semi1Δ* cells.

(I) Zfr3 does not localize to the MAC in *spo11Δ semi1i* cells.

(J) Semi1 localizes to the selected hMIC in *zfr3i* cells.

(K) Semi1 localizes to the MAC in *spo11Δ zfr3i* cells.

(F–K) Bottom: merged image. h: hMIC; yellow arrow: selected hMIC; †: degenerating unselected hMIC; arrowhead: gametic pronucleus; \$: progeny MAC; #: progeny MIC; dotted line: conjugation junction. Scale bar: 10 μ m.

in di- or tri-micronucleate *T. thermophila* mutants even though eight or 12 hMICs are generated by meiosis within a single cell (Nanney, 1953), suggesting that ciliates have the capability to ensure that only one hMIC undergoes post-meiotic development. The mechanism and reason for selecting a single hMIC from the meiotic products is unknown, but it may be important to cull the extra hMICs to prevent undesirable self-fertilization. The selection mechanism was previously assumed to target the hMIC located closest to or in contact with the conjugation junction after the second meiotic division (Gaertig and Fleury, 1992; Ishida et al., 1999; Numata et al., 1985; Takagi et al., 1991). This principle would resemble that of female meiosis in most flowering plants, in which only the meiotic product most proximal to the longitudinal axis of the ovule primordium is selected to become the functional megaspore (Demesa-Arevalo and Vielle-Calzada, 2013). However, the *semi1* mutation showed that in *T. thermophila* an hMIC that is not associated with the conjugation junction can be selected (Figure 3): on the contrary, hMIC attachment follows hMIC selection. Because MIC chromatin is symmetrically segregated to the hMICs during meiosis (Howard-Till and Loidl, 2018), (epi)genetic or physiological inequality between the meiotic products is unlikely to determine their different fates. This contrasts with female meiosis in animals, where asymmetric spindle formation produces big egg cells and small polar bodies (Clift and Schuh, 2013; Kursel and Malik, 2018).

In the absence of clear differences in the positions of hMICs (Figures 3D–3F), their different fates in WT cells may be due to a random process in which the arrival of the first hMIC in a suitable cellular location for selection to form a gametic pronucleus commits the other hMICs to autophagy. This situation resembles random X inactivation in female mammals, in which a signal from the active X chromosome (whose inactivation is prevented by blocking factors [Nicodemi and Prisco, 2007]) inactivates the other X chromosome (or chromosomes in triple-X cells) (Lu et al., 2017; Pollex and Heard, 2019). In this case, the inactivating signal is not a protein, which would have to be expressed by one of the X chromosomes and then translated and imported into the nucleus, where it would affect both X chromosomes similarly. Instead, the message may consist of non-coding RNA (Pollex and Heard, 2019). Although in *Tetrahymena* the source and recipient of the signal are not different chromosomes within a nucleus but different nuclei within a cell, we speculate that a similar principle could work in hMIC selection.

Semi1 Positions the Selected hMIC at the Conjugation Junction

Several lines of evidence indicate that microtubules form a meshwork around the conjugation junction to promote gametic pronuclear exchange (Orias et al., 1983; Kushida et al., 2015). This meshwork is also thought to be responsible for hMIC attachment to the conjugation junction by trapping the selected hMIC (Gaertig and Fleury, 1992). In addition to microtubules, a filament-forming citrate synthase, Cit1, also forms a meshwork around the conjugation junction (Numata et al., 1985; Takagi et al., 1991). Therefore, it is possible that Semi1 might utilize the polymerization or depolymerization forces of tubulin or Cit1 to move the selected hMIC toward the conjugation junction. Alternatively, Semi1 may interact with motor proteins or Rab GTPases to drive the movement of the selected hMIC along these filaments. However, contrary to our expectations, none of these proteins co-precipitated with Semi1 (Tables 1 and S1). This result suggests that Semi1-mediated hMIC attachment to the conjugation junction may bear little (or no) resemblance to the cytoskeleton-dependent nuclear positioning or membrane trafficking that occurs in other

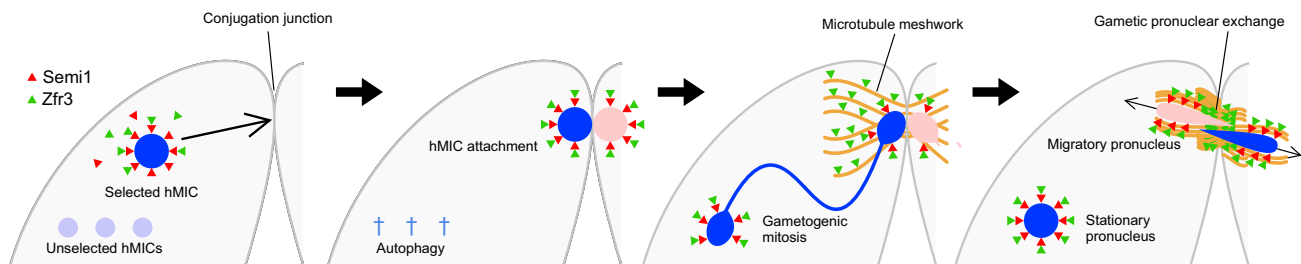


Figure 6. Model of Semi1 Recruitment of the Selected hMIC to the Conjugation Junction

Once an hMIC is selected at random (see also Figure S6), Semi1 binds to its rim. Semi1 recruits the selected hMIC to the conjugation junction to enable hMIC attachment to occur in a microtubule-independent manner. Semi1 also recruits Zfr3 to the surface of the selected hMIC. Zfr3 may interact with microtubules at the conjugation junction, and the Semi1–Zfr3 complex is responsible for pronuclear exchange.

organisms (Tran et al., 2001; Gundersen and Worman, 2013; Huelsmann and Brown, 2014; Kiral et al., 2018). It is also possible that Semi1 has a regulatory rather than an active role in cytoskeleton-dependent nuclear relocation.

Alternatively, the molecular affinity between Semi1 and proteins expressed at the conjugation junction may be sufficient to trap the selected hMIC. A previous proteomic analysis of isolated junctions from conjugating cells identified 15 proteins, including an epiplasmic protein (Cole et al., 2008). In addition, recent studies identified a fusogen protein Hap2, a homolog of male-gamete-specific protein (Cole et al., 2014; Pinello et al., 2017), and a zinc finger protein Zfr1 (Xu et al., 2012), both of which are essential components of the conjugation junction. One of the 15 proteins, Ftt18, was originally discovered as a basal body component (Kilburn et al., 2007). It was also identified as a Semi1 interactor in our experiments (Table S1) and localized to both the conjugation junction and the periphery of the selected hMIC (Figure S4). Unfortunately, the mutant phenotype could not be studied owing to technical issues. However, it remains possible that interaction (direct or indirect) between Semi1 and Ftt18 is sufficient to bind an hMIC to the conjugation junction once it comes into close proximity. This suggests a model for hMIC selection in which all hMICs have the potential to pass close to the conjugation junction by random movement, but only a nucleus with the appropriate membrane makeup (the selected hMIC or in some cases the MAC) would become trapped there.

Markers on the Nuclear Surface May Determine the hMIC Position

A hMIC may acquire some similar properties to the MAC upon nuclear fate determination (Figures 4A–4C), which may guide Semi1 to the periphery of selected hMIC to ensure hMIC attachment. In fact, in the selected hMIC histone H3 is acetylated at several lysine residues (Akematsu et al., 2017) other than K56 (Figure 3A). Acetylation of histone H3 at these sites is strongly enriched in euchromatin (Wang et al., 2008; Tie et al., 2009) and also characteristic of the active MAC (Chicoine and Allis, 1986; Pfeffer et al., 1989). This change may also be critical to protect the selected hMIC from autophagy, which eliminates the unselected hMICs (Liu and Yao, 2012). The first hMICs to come into contact with the MAC may undergo changes that cause its membrane properties to resemble those of the MAC, which leads to changes in the chromatin, resulting in selection. We showed that perinuclear Semi1 contributes to nuclear migration toward the conjugation junction (Figures 2A and 4A), probably without a direct interaction with microtubules or motor proteins (Table 1). Similar functional relationships between surface markers and the characteristic internuclear mobility may be general features of mating *T. thermophila* cells. For instance, the degenerating parental MAC migrates toward the posterior of the cell (Cole and Sugai, 2012). The surface of this nucleus is decorated with glycocalyx compounds and phosphatidylserine, which are absent from the other nuclei within the cell, and may be recognized by the autophagic machinery (Akematsu et al., 2010). Similarly, the unselected hMICs migrate to the posterior region of the cell (Cole and Sugai, 2012). Although the direct relevance of this surface property to nuclear migration is unknown, loss of autophagy-related genes prevents migration and, hence, lysosomal acidification of the nucleus (Liu and Yao, 2012; Akematsu et al., 2014). Different nuclear surface molecules may therefore be recognized by different intracellular trafficking pathways so as to guide the different nuclei to specific cell compartments where they are differentially processed.

Limitations of the Study

Owing to limited experimental conditions and equipment, we were unable to perform time-lapse imaging to capture hMIC selection in live cells. Also, topology of Semi1 in the nuclear membrane is unclear because a reliable topology prediction tool is currently unavailable for the nuclear envelope proteins.

METHODS

All methods can be found in the accompanying [Transparent Methods supplemental file](#).

SUPPLEMENTAL INFORMATION

Supplemental Information can be found online at <https://doi.org/10.1016/j.isci.2019.100749>.

ACKNOWLEDGMENTS

We thank Masaaki Iwamoto for providing GFP-Nup93-expressing *T. thermophila* strains and Marcella D. Cervantes for providing information on mating-type-specific primers. We acknowledge the support of Miao Tian, Yasuhiro Fukuda, Markus Hartl, and Thomas Gossenreiter in co-immunoprecipitation and MS experiments. This research was funded by a Mahlke-Obermann Stiftung grant and the European Union's Seventh Framework Programme for Research, Technological Development, and Demonstration (grant no. 609431) to T.A. and an Austrian Science Fund (FWF) grant (P27313-B20) to J.L.

AUTHOR CONTRIBUTIONS

T.A. designed and performed most of the experiments and wrote the manuscript. R.S-F performed the co-immunoprecipitation, data analysis of mass spectrometry, and *semi1*Δ rescue experiment. F.K. performed the Zfr3 localization and knockdown experiments. E.H. performed the Semi1 truncation and mutation experiments. J.L. created the *semi1*Δ strains, contributed to the experimental design, and reviewed the manuscript.

DECLARATION OF INTERESTS

The authors declare no competing interests.

Received: September 10, 2019

Revised: November 1, 2019

Accepted: November 25, 2019

Published: January 24, 2020

REFERENCES

- Akematsu, T., Fukuda, Y., Attiq, R., and Pearlman, R.E. (2014). Role of class III phosphatidylinositol 3-kinase during programmed nuclear death of *Tetrahymena thermophila*. *Autophagy* 10, 209–225.
- Akematsu, T., Fukuda, Y., Garg, J., Fillingham, J.S., Pearlman, R.E., and Loidl, J. (2017). Post-meiotic DNA double-strand breaks occur in *Tetrahymena*, and require Topoisomerase II and Spo11. *Elife* 6, e26176.
- Akematsu, T., Pearlman, R.E., and Endoh, H. (2010). Gigantic macroautophagy in programmed nuclear death of *Tetrahymena thermophila*. *Autophagy* 6, 901–911.
- Chen, C.C., Carson, J.J., Feser, J., Tamburini, B., Zabaronick, S., Linger, J., and Tyler, J.K. (2008). Acetylated lysine 56 on Histone H3 drives chromatin assembly after repair and signals for the completion of repair. *Cell* 134, 231–243.
- Chicoine, L.G., and Allis, C.D. (1986). Regulation of histone acetylation during macronuclear differentiation in *Tetrahymena*: evidence for control at the level of acetylation and deacetylation. *Dev. Biol.* 116, 477–485.
- Chowdhury, D., Keogh, M.C., Ishii, H., Peterson, C.L., Buratowski, S., and Lieberman, J. (2005). gamma-H2AX dephosphorylation by protein phosphatase 2A facilitates DNA double-strand break repair. *Mol. Cell* 20, 801–809.
- Clift, D., and Schuh, M. (2013). Restarting life: fertilization and the transition from meiosis to mitosis. *Nat. Rev. Mol. Cell Biol.* 14, 549–562.
- Cole, E., and Sugai, T. (2012). Developmental progression of *Tetrahymena* through the cell cycle and conjugation. *Methods Cell Biol.* 109, 177–236.
- Cole, E.S., Anderson, P.C., Fulton, R.B., Majerus, M.E., Rooney, M.G., Savage, J.M., Chalker, D., Honts, J., Welch, M.E., Wentland, A.L., et al. (2008). A proteomics approach to cloning fenestrin from the nuclear exchange junction of *tetrahymena*. *J. Eukaryot. Microbiol.* 55, 245–256.
- Cole, E.S., Cassidy-Hanley, D., Fricke Pinello, J., Zeng, H., Hsueh, M., Kolbin, D., Ozzello, C., Giddings, T., Jr., Winey, M., and Clark, T.G. (2014). Function of the male-gamete-specific fusion protein HAP2 in a seven-sexed ciliate. *Curr. Biol.* 24, 2168–2173.
- Demasa-Arevalo, E., and Vielle-Calzada, J.P. (2013). The classical arabinogalactan protein AGP18 mediates megaspore selection in *Arabidopsis*. *Plant Cell* 25, 1274–1287.
- Fu, H., Subramanian, R.R., and Masters, S.C. (2000). 14-3-3 proteins: structure, function, and regulation. *Annu. Rev. Pharmacol. Toxicol.* 40, 617–647.
- Gaertig, J., and Fleury, A. (1992). Spatio-temporal reorganization of intracytoplasmic microtubules is associated with nuclear selection and differentiation during the developmental process in the ciliate *Tetrahymena thermophila*. *Protoplasma* 167, 74–87.
- Gao, X., Zhang, X., and Yang, X. (2010). Morphological apoptotic characteristics of the

- post-meiotic micronuclei in *Paramecium caudatum*. *Eur. J. Protistol.* **46**, 243–250.
- Garnier, O., Serrano, V., Duhaucourt, S., and Meyer, E. (2004). RNA-mediated programming of developmental genome rearrangements in *Paramecium tetraurelia*. *Mol. Cell. Biol.* **24**, 7370–7379.
- Gundersen, G.G., and Worman, H.J. (2013). Nuclear positioning. *Cell* **152**, 1376–1389.
- Hayashi, A., and Mochizuki, K. (2015). Targeted gene disruption by ectopic induction of DNA elimination in *Tetrahymena*. *Genetics* **201**, 55–64.
- Howard-Till, R., and Loidl, J. (2018). Condensins promote chromosome individualization and segregation during mitosis, meiosis, and amitosis in *Tetrahymena thermophila*. *Mol. Biol. Cell* **29**, 466–478.
- Huelsmann, S., and Brown, N.H. (2014). Nuclear positioning by actin cables and perinuclear actin: special and general? *Nucleus* **5**, 219–223.
- Ishida, M., Nakajima, Y., Kurokawa, K., and Mikami, K. (1999). Nuclear behavior and differentiation in *Paramecium caudatum*, analyzed by immunofluorescence with anti-tubulin antibody. *Zoolog. Sci.* **16**, 915–927.
- Iwamoto, M., Mori, C., Kojidani, T., Bunai, F., Hori, T., Fukagawa, T., Hiraoka, Y., and Haraguchi, T. (2009). Two distinct repeat sequences of Nup98 nucleoporins characterize dual nuclei in the binucleated ciliate tetrahymena. *Curr. Biol.* **19**, 843–847.
- Kadoch, C., and Crabtree, G.R. (2015). Mammalian SWI/SNF chromatin remodeling complexes and cancer: mechanistic insights gained from human genomics. *Sci. Adv.* **1**, e1500447.
- Kilburn, C.L., Pearson, C.G., Romijn, E.P., Meehl, J.B., Giddings, T.H., Jr., Culver, B.P., Yates, J.R., 3rd, and Winey, M. (2007). New *Tetrahymena* basal body protein components identify basal body domain structure. *J. Cell Biol.* **178**, 905–912.
- Kiral, F.R., Kohrs, F.E., Jin, E.J., and Hiesinger, P.R. (2018). Rab GTPases and membrane trafficking in neurodegeneration. *Curr. Biol.* **28**, R471–R486.
- Komori, R., Harumoto, T., Fujisawa, H., and Takagi, Y. (2004). A *Paramecium tetraurelia* mutant that has long autogamy immaturity period and short clonal life span. *Mech. Ageing Dev.* **125**, 603–613.
- Kursel, L.E., and Malik, H.S. (2018). The cellular mechanisms and consequences of centromere drive. *Curr. Opin. Cell Biol.* **52**, 58–65.
- Kushida, Y., Takaine, M., Nakano, K., Sugai, T., and Numata, O. (2015). Dynamic change of cellular localization of microtubule-organizing center during conjugation of ciliate *Tetrahymena thermophila*. *Zool. Sci.* **32**, 25–32.
- Liu, M.L., and Yao, M.C. (2012). Role of ATG8 and autophagy in programmed nuclear degradation in *Tetrahymena thermophila*. *Eukaryot. Cell* **11**, 494–506.
- Lu, Z., Carter, A.C., and Chang, H.Y. (2017). Mechanistic insights in X-chromosome inactivation. *Philos. Trans. R. Soc. Lond. B Biol. Sci.* **372**, 20160356.
- Miao, W., Xiong, J., Bowen, J., Wang, W., Liu, Y., Braguinets, O., Grigull, J., Pearlman, R.E., Orias, E., and Gorovsky, M.A. (2009). Microarray analyses of gene expression during the *Tetrahymena thermophila* life cycle. *PLoS One* **4**, e4429.
- Nanney, D.L. (1953). Nucleo-cytoplasmic interaction during conjugation in *Tetrahymena*. *Biol. Bull.* **105**, 133–148.
- Nanney, D.L., and Nagel, M.J. (1964). Nuclear misbehavior in an aberrant inbred *Tetrahymena*. *J. Protozool.* **11**, 465–473.
- Nicodemi, M., and Prisco, A. (2007). Self-assembly and DNA binding of the blocking factor in x chromosome inactivation. *PLoS Comput. Biol.* **3**, e210.
- Numata, O., Sugai, T., and Watanabe, Y. (1985). Control of germ cell nuclear behaviour at fertilization by *Tetrahymena* intermediate filament protein. *Nature* **314**, 192–194.
- Orias, E., Cervantes, M.D., and Hamilton, E.P. (2011). *Tetrahymena thermophila*, a unicellular eukaryote with separate germline and somatic genomes. *Res. Microbiol.* **162**, 578–586.
- Orias, J.D., Hamilton, E.P., and Orias, E. (1983). A microtubule meshwork associated with gametic pronucleus transfer across a cell-cell junction. *Science* **222**, 181–184.
- Pfeffer, U., Ferrari, N., Tosetti, F., and Vidali, G. (1989). Histone acetylation in conjugating *Tetrahymena thermophila*. *J. Cell Biol.* **109**, 1007–1014.
- Pinello, J.F., Lai, A.L., Millet, J.K., Cassidy-Hanley, D., Freed, J.H., and Clark, T.G. (2017). Structure-function studies link class II viral fusogens with the ancestral gamete fusion protein HAP2. *Curr. Biol.* **27**, 651–660.
- Pollex, T., and Heard, E. (2019). Nuclear positioning and pairing of X-chromosome inactivation centers are not primary determinants during initiation of random X-inactivation. *Nat. Genet.* **51**, 285–295.
- Prescott, D.M. (1994). The DNA of ciliated protozoa. *Microbiol. Rev.* **58**, 233–267.
- Shang, Y., Song, X., Bowen, J., Corstanje, R., Gao, Y., Gaertig, J., and Gorovsky, M.A. (2002). A robust inducible-repressible promoter greatly facilitates gene knockouts, conditional expression, and overexpression of homologous and heterologous genes in *Tetrahymena thermophila*. *Proc. Natl. Acad. Sci. U S A* **99**, 3734–3739.
- Shi, L., and Oberdoerffer, P. (2012). Chromatin dynamics in DNA double-strand break repair. *Biochim. Biophys. Acta* **1819**, 811–819.
- Takagi, I., Numaka, O., and Watanabe, Y. (1991). Involvement of 14-nm filament-forming protein and tubulin in gametic pronuclear behavior during conjugation in *Tetrahymena*. *J. Eukaryot. Microbiol.* **38**, 345–351.
- Teo, G., Liu, G., Zhang, J., Nesvizhskii, A.I., Gingras, A.C., and Choi, H. (2014). SAINTexpress: improvements and additional features in Significance Analysis of INteractome software. *J. Proteomics* **100**, 37–43.
- Tie, F., Banerjee, R., Stratton, C.A., Prasad-Sinha, J., Stepanik, V., Zlobin, A., Diaz, M.O., Scacheri, P.C., and Harte, P.J. (2009). CBP-mediated acetylation of histone H3 lysine 27 antagonizes *Drosophila* Polycomb silencing. *Development* **136**, 3131–3141.
- Tran, P.T., Marsh, L., Doye, V., Inoue, S., and Chang, F. (2001). A mechanism for nuclear positioning in fission yeast based on microtubule pushing. *J. Cell Biol.* **153**, 397–411.
- Wang, Z., Zang, C., Rosenfeld, J.A., Schones, D.E., Barski, A., Cuddapah, S., Cui, K., Roh, T.Y., Peng, W., Zhang, M.Q., and Zhao, K. (2008). Combinatorial patterns of histone acetylations and methylations in the human genome. *Nat. Genet.* **40**, 897–903.
- Woehrer, S.L., Aronica, L., Suhren, J.H., Busch, C.J., Noto, T., and Mochizuki, K. (2015). A *Tetrahymena* Hsp90 co-chaperone promotes siRNA loading by ATP-dependent and ATP-independent mechanisms. *EMBO J.* **34**, 559–577.
- Xu, J., Tian, H., Wang, W., and Liang, A. (2012). The zinc finger protein Zfr1p is localized specifically to conjugation junction and required for sexual development in *Tetrahymena thermophila*. *PLoS One* **7**, e52799.
- Yanagi, A. (1987). Positional control of the fates of nuclei produced after meiosis in *Paramecium caudatum*: analysis by nuclear transplantation. *Dev. Biol.* **122**, 535–539.

ISCI, Volume 23

Supplemental Information

The Transmembrane Protein Semi1

Positions Gamete Nuclei

for Reciprocal Fertilization in *Tetrahymena*

Takahiko Akematsu, Rosalía Sánchez-Fernández, Felix Kosta, Elisabeth Holzer, and Josef Loidl

Supplemental information

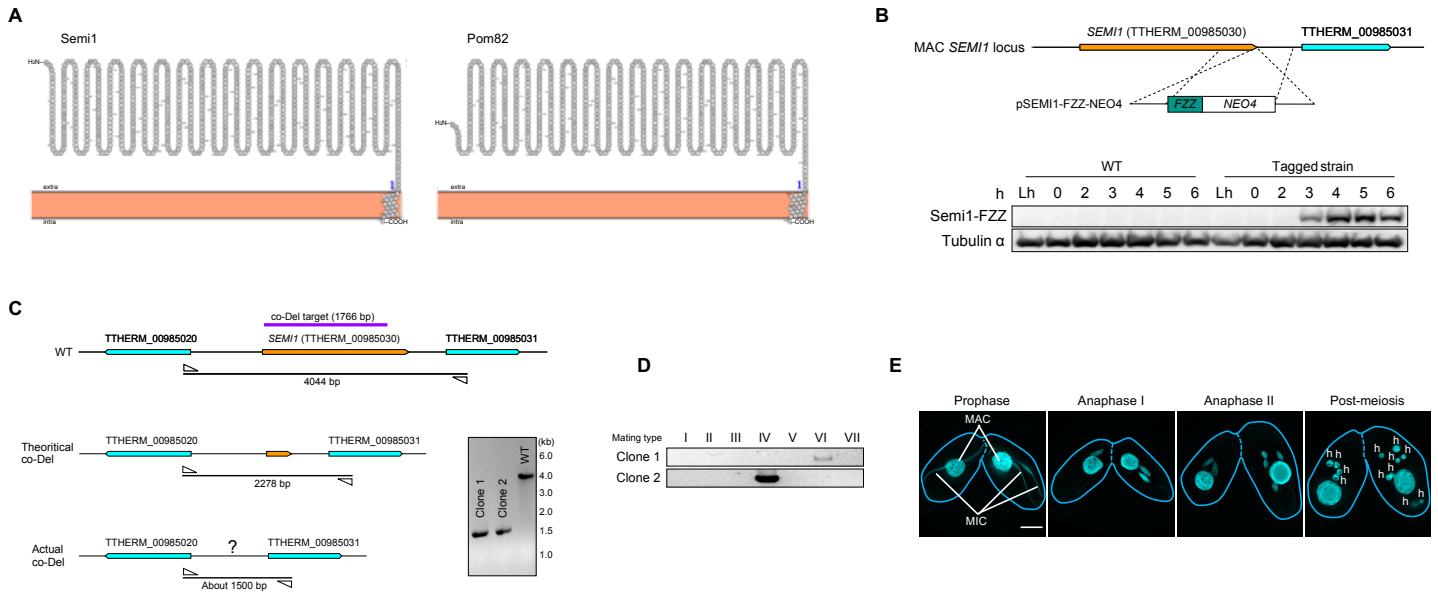


Figure S1. Characterization of Semi1 and generation of somatic *semi1* knockout mutants. Related to Figure 1.

(A) Possible topologies of the Semi1 (left) and the Pom82 (right) proteins in the MIC envelope. Pom82 is a transmembrane nucleopore present in the MIC (Iwamoto et al., 2017). Since topology prediction tools specialized for nuclear envelope proteins do not exist, we used PROTTER (<http://wlab.ethz.ch/protter/start/>), an open source tool for visualization of general transmembrane topology, to predict Semi1's orientation in the MIC envelope. The orange bars represent cell membrane. As seen in Pom82, the C-terminal and the other regions of Semi1 were predicted to be a transmembrane domain and to face extracellular space, respectively. This result suggests that the non-transmembrane region of Semi1 is exposed to the cytosol as of Pom82. (B) Construction of FZZ-tagged Semi1-expressing cells. The pSEMI1-FZZ-NEO4 plasmid, containing an FZZ tag and neomycin resistance cassette (*NEO4*), was integrated into the MAC *SEMI1* locus by homologous recombination. Conjugation-specific expression of FZZ-tagged Semi1 was confirmed by western blotting. Cells were collected at the indicated times after the initiation of conjugation. Lh: exponentially growing cells; 0: starved cells. Tubulin α was the loading control. (C) Generation of *semi1* Δ cells and PCR confirmation. PCR primers are indicated by white triangles. The WT *SEMI1* genomic locus (1766 bp, indicated by purple line) was targeted by the co-Del plasmid. A DNA fragment of 2278 bp is expected from co-Del cells. However, fragments were about 1500 bp, indicating deletion of flanking regions. (D) Mating types of the *semi1* Δ clones were determined by PCR using mating-type-specific primer sets (gift from Dr Marcella D. Cervantes, Albion College, MI, USA). (E) Induction of meiosis in the unexchanged gametic pronuclei of *semi1* Δ exconjugant (see also Figure 1B). A *semi1* Δ exconjugant (right) mated with a parental *semi1* Δ cell (left) was stained with DAPI. The unexchanged gametic pronuclei in right cell became eight meiotic products, the number of which is twice as many as the left cell, suggesting that *semi1* Δ exconjugants undergo DNA endoreplication in the unexchanged gametic pronuclei prior to the next round of meiosis. h: hMICs. Dotted line: conjugation junction. Scale bar: 10 μ m.

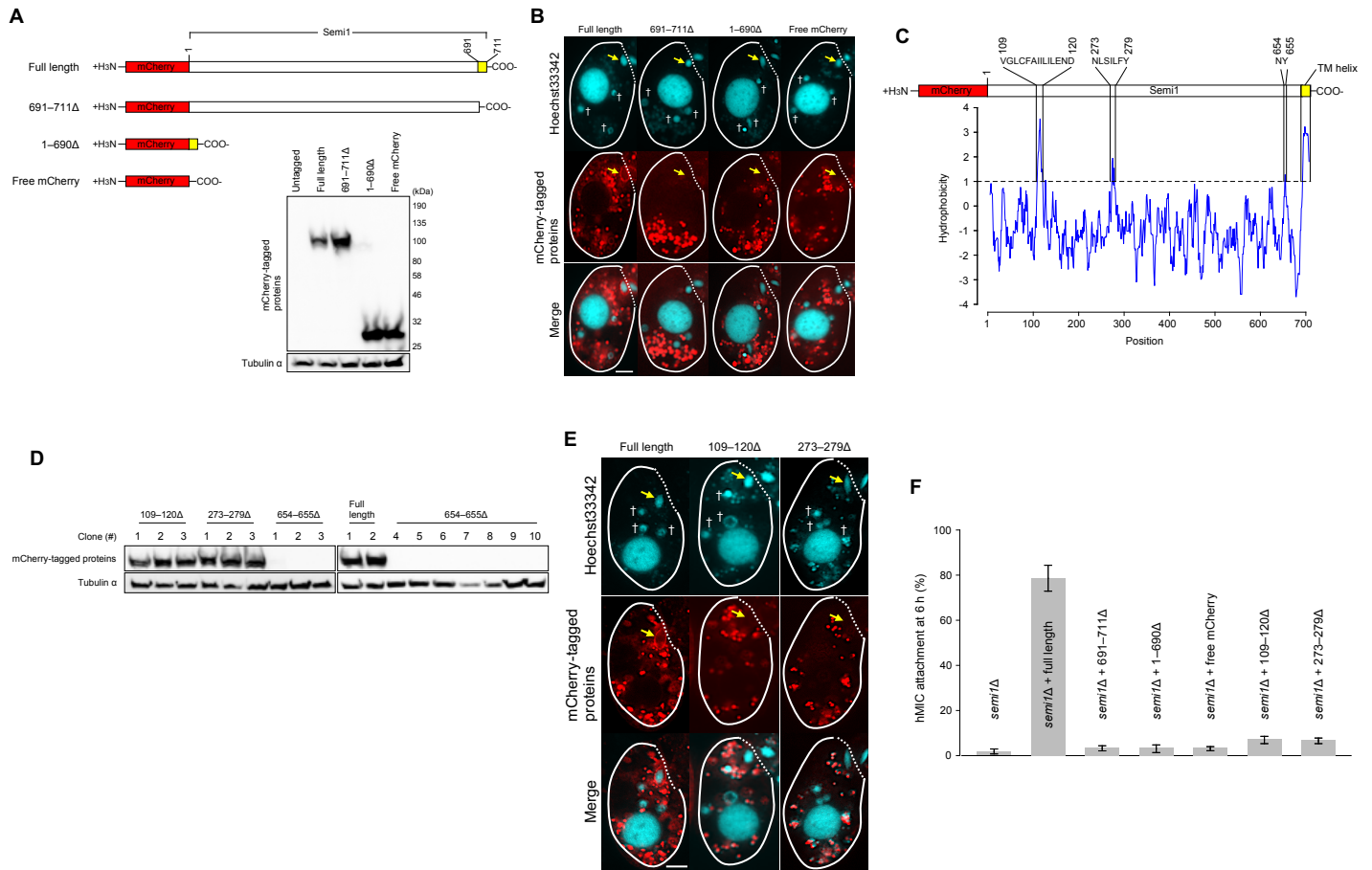


Figure S2. Perinuclear localization of Semi1 mediates hMIC attachment to the conjugation junction. Related to Figure 1.

(A) Schematic representation of full-length mCherry-Semi1 and truncated variants. The yellow box represents the transmembrane helix. Western blot was used to confirm protein expression. Tubulin α was the loading control. (B) Truncated mCherry-Semi1 variants do not localize to the perinuclear region. Hoechst 33342 staining shows the position of the MAC and hMICs in living cells was. Arrowhead: selected hMIC; †: degenerating unselected hMIC. Dotted line: conjugation junction. Scale bar: 10 μ m. (C) A schematic diagram showing the hydrophobic regions of Semi1, as profiled by ProtScale (<https://web.expasy.org/protscale/>). The three non-transmembrane regions (109–120, 273–279, and 654–655) were deleted from the mCherry-Semi1 expression construct. TM: transmembrane. (D) Western blotting analysis of the expression of mCherry-Semi1 deletion variants. Expression of variant 654–655 Δ was undetectable in 10 different clones, indicating that residues N654 and Y655 are important for protein stability. (E) mCherry-Semi1 variants lacking the transmembrane region fail to localize to the perinuclear region of the selected hMIC. Arrowhead: selected hMIC; †: degenerating unselected hMIC. Dotted line: conjugation junction. Scale bar: 10 μ m. (F) Percentage of cells with normal hMIC attachment to the conjugation junction at 6 h after the initiation of conjugation. The truncated variants and the deleted versions of mCherry-Semi1 were expressed in *semi1Δ* cells. Columns and error bars represent means and standard deviations of three measurements.

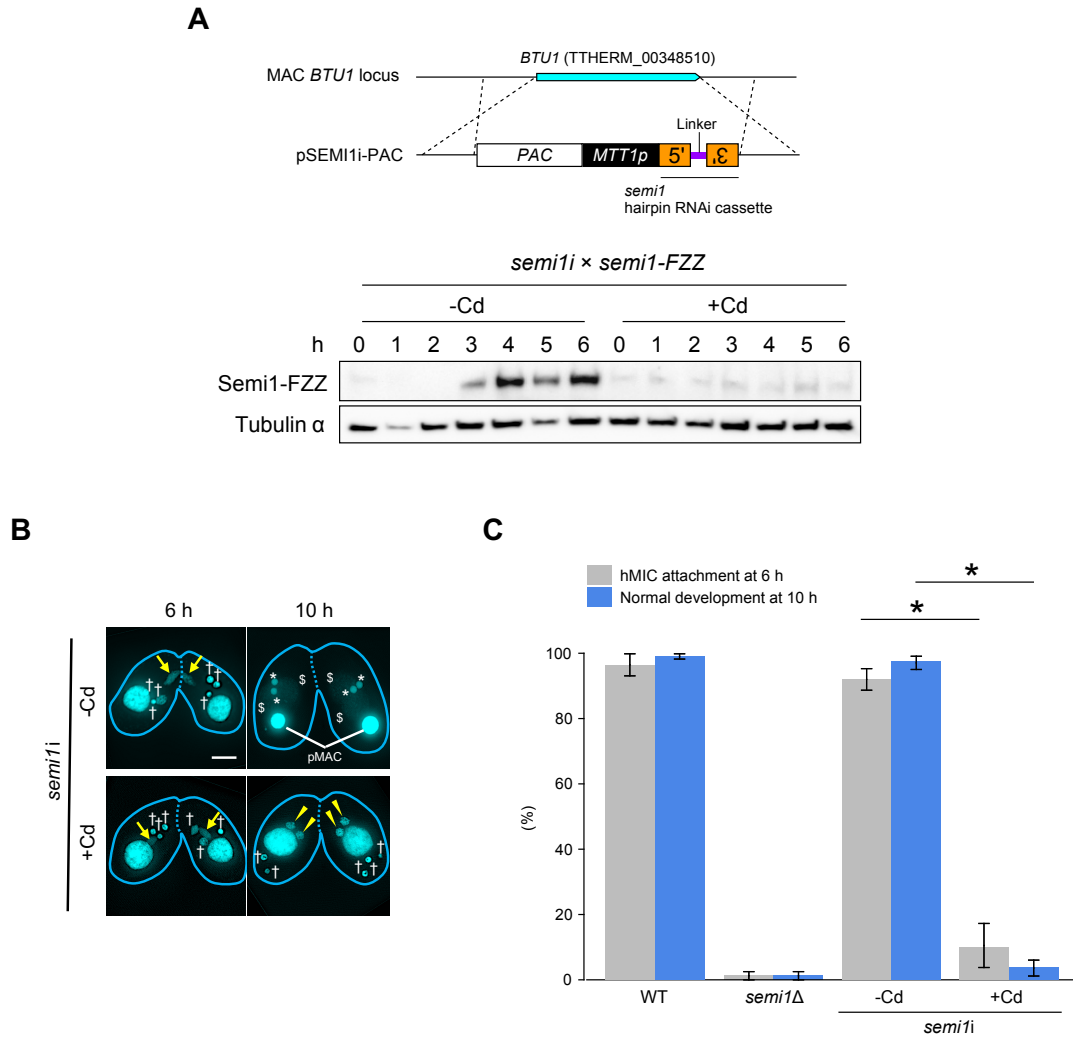


Figure S3. *semi1* RNAi expression has the same phenotype as the *semi1Δ* mutant. Related to Figure 4.

(A) Generation of *semi1i*-expressing cells. The pSEMI1i-PAC plasmid, containing a puromycin resistance marker (*PAC*), cadmium-inducible *MTT1* promoter, and hairpin RNAi cassette, was integrated into the MAC *BTU1* locus of Semi1-FZZ-expressing cells by homologous recombination. Western blotting confirms that Semi1-FZZ expression is lost following *semi1* RNAi induction. Tubulin α was the loading control. (B) Cells expressing *semi1i* had the same phenotype as *semi1Δ* cells at 6 h and 10 h after the expression of RNAi. Arrow: selected hMIC undergoing gametogenic mitosis; †: degenerating unselected hMIC; arrowhead: gametic pronucleus; \$: progeny MAC; #: progeny MIC. Dotted line: conjugation junction. Scale bar: 10 μm. (C) Percentage of cells with normal hMIC attachment at 6 h after the initiation of conjugation and with normal development of progeny nuclei at 10 h. Columns and error bars represent the means and standard deviations of three independent experiments. Asterisk (*) shows a significant differences between columns ($p < 0.01$, as calculated by Tukey's HSD test on RStudio).

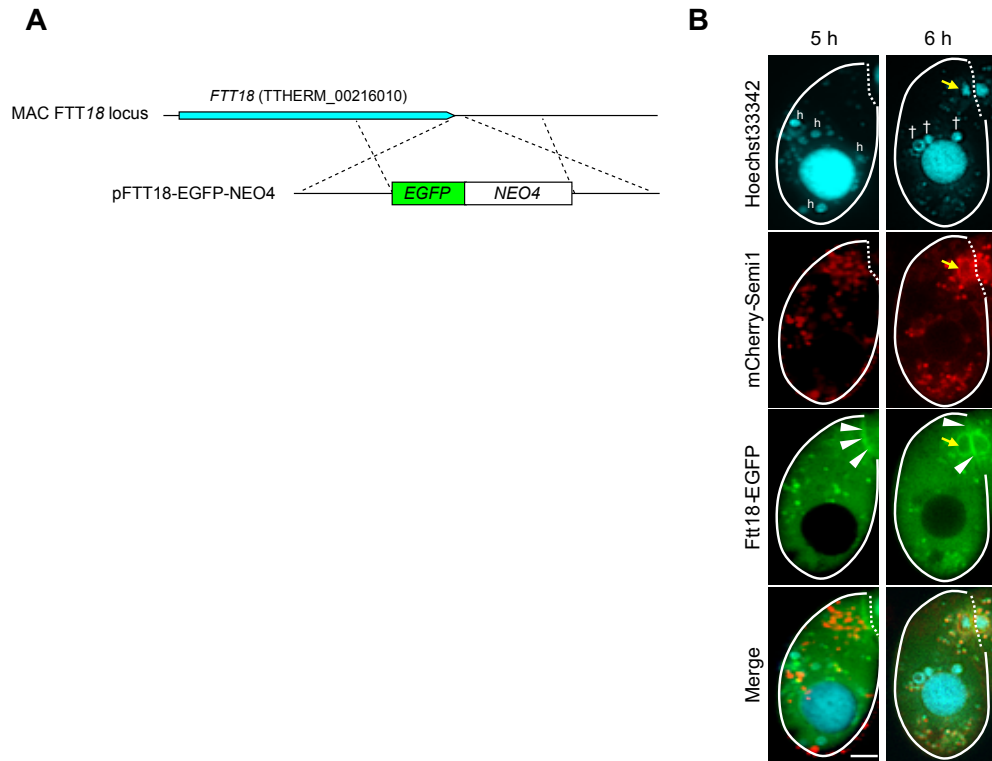


Figure S4. Ftt18 localizes to both the conjugation junction and the selected hMIC. Related to Table 1.

(A) Generation of cells expressing EGFP-tagged Ftt18. The pFTT18-EGFP-NEO4 plasmid, containing an *EGFP* tag and neomycin resistance cassette (*NEO4*), was integrated into the MAC *FTT18* locus by homologous recombination. (B) Ftt18-EGFP (arrowheads) localizes to the conjugation junction at 5 h after the initiation of conjugation and co-localizes with mCherry-Semi1 to the selected hMIC (arrow). h: hMIC; †: degenerating unselected hMIC. Dotted line: conjugation junction. Scale bar: 10 μ m.

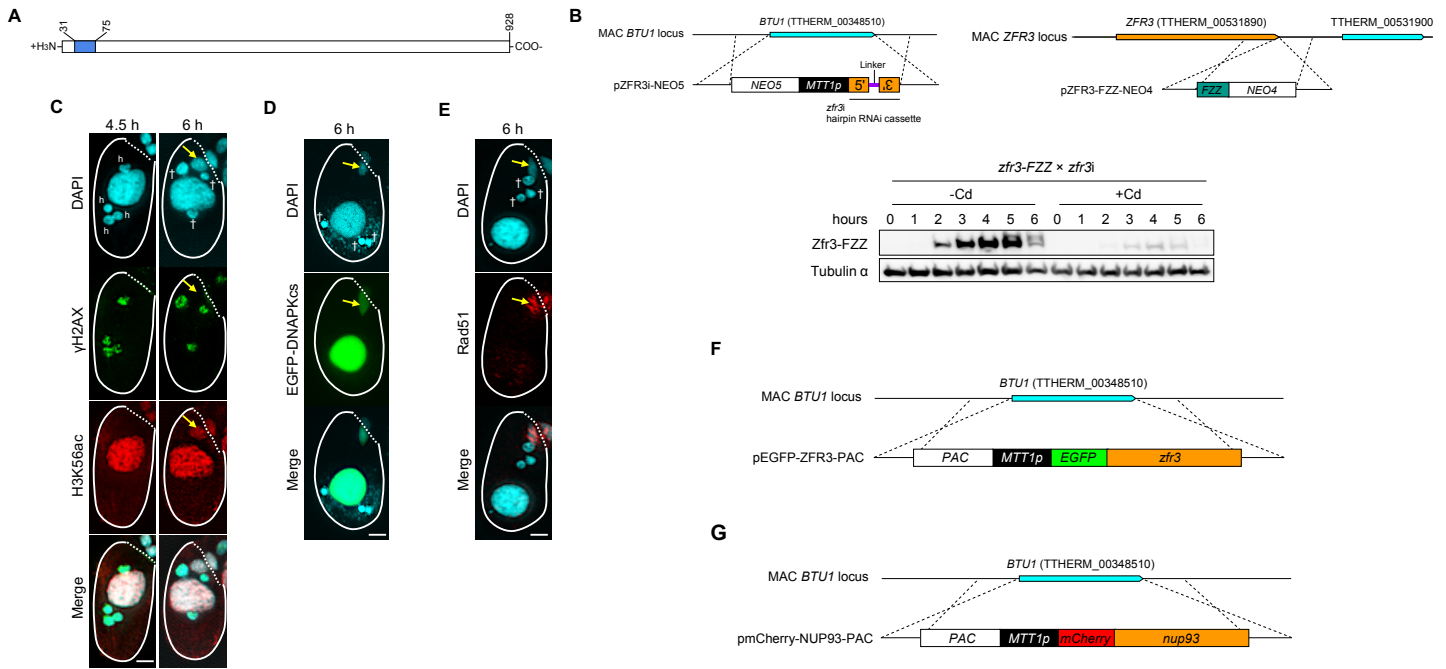


Figure S5. RNAi-mediated knockdown of the *Zfr3* conjugation-specific protein. Related to Figure 5.

(A) Primary structure of the *Zfr3* protein. No homolog has been found in other organisms. The blue box represents a C3HC4 type zinc finger domain. (B) Generation of cell lines expressing a *zfr3* RNAi (*zfr3i*) (upper left) and FZZ-tagged *Zfr3* (upper right). The pZFR3i-NEO5 plasmid, containing a paromomycin resistance marker (*NEO5*), cadmium-inducible *MTT1* promoter, and hairpin RNAi cassette, or the pZFR3-FZZ-NEO4 plasmid, containing a FZZ tag and neomycin resistance cassette (*NEO4*), were integrated into the MAC *BTU1* locus or the MAC *ZFR3* locus, respectively, by homologous recombination. The resulting cell lines were mated, and protein was extracted. Western blotting showed that *Zfr3*-FZZ expression is strongly reduced upon *zfr3i* induction. Tubulin α was the loading control. (C) γ H2AX localizes to all four hMICs at 4.5 h after the initiation of conjugation in *zfr3i* cells. At 6 h, one hMIC (arrow) loses γ H2AX staining concomitant with histone H3 acetylation at lysine 56 (H3K56ac). h: hMIC; †: degenerating unselected hMIC. Dotted line: conjugation junction. Scale bars: 10 μ m. (D) EGFP-tagged DNAPKcs localizes to the hMIC nearest to the conjugation junction (arrow) in *zfr3i* cells at 6 h after the initiation of conjugation. †: degenerating unselected hMIC. Dotted line: conjugation junction. Scale bars: 10 μ m. (E) Rad51 localizes to the hMIC nearest to the conjugation junction (arrow) in *zfr3i* cells. †: degenerating unselected hMIC. Dotted line: conjugation junction. Scale bars: 10 μ m. (F) Generation of a cell line expressing EGFP-tagged *Zfr3*. The pEGFP-ZFR3-PAC plasmid, containing a puromycin resistance marker (*PAC*), cadmium-inducible *MTT1* promoter, and EGFP-*Zfr3* expression cassette, was integrated into the MAC *BTU1* locus by homologous recombination. (G) Generation of a cell line expressing mCherry-tagged NUP93. The pmCherry-ZFR-PAC plasmid, containing a puromycin resistance marker (*PAC*), cadmium-inducible *MTT1* promoter, and EGFP-*Zfr3* expression cassette, was integrated into the MAC *BTU1* locus by homologous recombination.

Table S1. MS identification of constitutively expressed interaction partners of Semi1. Related to Table 1.

Gene ID (THERM_)	AvgCount	Control count	p-value	Protein name	Description
00216010	133.5	0 4	0	Ftt18	14-3-3 protein
00194540	81	4 6	0	None	TATA-binding protein interacting (TIP20) protein
00105110	61	7 12	0	Hsp70	HSP70 heat shock 70 kDa protein
00158520	43.5	3 2	0	Hsp82	HSP82 predicted protein
00161720	41	0 0	0	None	Zinc finger in N-recognin family protein
00579319	35.5	0 0	0	None	Hypothetical protein
00160770	35	0 1	0	Ftt49	14-3-3 protein
00535500	32	0 1	0	None	DnaJ domain protein
00047040	29	0 0	0	None	Ubiquitin carboxy-terminal hydrolase
00550700	25.5	0 2	0	None	Importin protein
00299570	24.5	0 3	0	None	Pyridine nucleotide-disulfide oxidoreductase
00865270	24.5	1 3	0	Ydj1	DnaJ carboxy-terminal domain protein
000522989	21	0 0	0	None	Hypothetical protein
00339610	20	1 4	0	Rpn1	RPN1 26S proteasome regulatory subunit
00444670	20	1 0	0	Hsp90	HSC82 heat shock protein HSP90
00476820	20	0 0	0	Rvb1	RVB holliday junction ATP-dependent DNA helicase RuvB
00138370	17.5	0 2	0	Atg7	ATG7 ubiquitin-like modifier-activating enzyme
00471950	17.5	1 0	0	None	Hypothetical protein
00891190	17.5	0 1	0	None	Hypothetical protein
00780580	17	0 5	0	Cyc16	CYC16 amine-terminal domain cyclin
00049030	16.5	0 0	0	None	Na,H/K antiporter P-type ATPase, alpha subunit family protein
00591660	16.5	0 0	0	None	Importin-beta amine-terminal domain protein
00502340	15.5	0 0	0	None	Glycerol-3-phosphatase 0-acyltransferase
001014659	15.5	0 5	0.01	None	26S proteasome regulatory complex ATPase RPT2
00068110	15.5	1 6	0.03	Rpt3	RPT3 26S protease regulatory subunit 6B
00627000	14.5	0 0	0	None	SIT4 Phosphatase-associated protein
00372460	14	0 0	0	Flp10	Phospholipid-translocating P-type ATPase, flippase family protein
00426310	14	0 3	0	None	Chaperone DnaJ
00771980	13	0 1	0	None	Tetratricopeptide repeat protein
00444500	12	0 0	0	Gcn1	HEAT repeat protein
00856430	12	0 0	0	None	E1-E2 ATPase family protein
00279670	12	0 4	0.01	Rpt1	RPT1 26S proteasome regulatory subunit
00158000	10	0 0	0	None	Transmembrane protein putative
00354810	10	0 0	0	None	Acyltransferase
00313530	10	0 3	0.01	None	Transmembrane protein putative
00657230	9	0 1	0	None	Hypothetical protein
00191240	9	1 4	0.02	Rpn7	RPN7 26S proteasome non-ATPase regulatory subunit 6
00578940	9	0 4	0.04	Rpn5	RPN5 26S proteasome non-ATPase regulatory subunit
01049200	9	0 4	0.04	None	Glutamate/leucine/phenylalanine/valine dehydrogenase
00011220	8.5	0 1	0	None	Kinase domain protein
00703480	8	0 0	0	None	Transmembrane protein putative
01084370	8	0 0	0	Tpa8	TPA8 sarco/endoplasmic reticulum calcium-translocating P-type ATPase
00047110	7	0 1	0	Alg5	ALG5 dolichyl-phosphate beta-glucosyltransferase
00437670	6.5	0 0	0	None	DnaJ domain protein

Transparent Methods

Culture methods and the induction of cell mating (conjugation)

WT *T. thermophila* strains CU428.2 (mating type VII, RRID:TSC_SD00178) and B2086 (mating type II, RRID:TSC_SD01627) were obtained from the *Tetrahymena* Stock Center, Cornell University (<http://tetrahymena.vet.cornell.edu/>). The GFP-Nup93-expressing strain (Iwamoto et al., 2009) was a gift from Dr Masaaki Iwamoto (Advanced ICT Research Institute, Kobe, Japan). Strains expressing EGFP-DNAPKcs (Akematsu et al., 2017) and *spo11Δ* (Mochizuki et al., 2008) were constructed previously. Cells were grown at 30°C in super proteose peptone (SPP) medium containing 1% proteose peptone (Becton Dickinson, Sparks, MD, USA), 0.1% yeast extract (Becton Dickinson), 0.2% glucose (Sigma-Aldrich, St. Louis, MO, USA), and 0.003% EDTA-Fe (Sigma-Aldrich). To make them competent for mating, cells at mid-log phase (approximately 10⁶ cells/mL) were washed with 10 mM Tris-HCl (pH7.4), resuspended in 10 mM Tris-HCl (pH7.4), and starved at 30°C for ~16 h. To induce mating, equal numbers of cells of two different mating types were mixed together and incubated at 30°C.

semi1 gene disruption

A 1776-bp fragment of the *SEMI1* open reading frame (ORF) was amplified from CU428.2 genomic DNA using PrimeSTAR Max DNA polymerase (TaKaRa, Kusatsu, Japan, Cat. R045A) and primers #1 and #2 (see below). The amplified fragment was cloned into the NotI site of the pMcoDel plasmid (Hayashi and Mochizuki, 2015) using the NEBuilder HF DNA Assembly kit (New England Biolabs, Ipswich, MA, USA, Cat. E5520S). NEB 5-alpha competent *E. coli* cells (New England Biolabs, Cat. C29871) were used to amplify all plasmids created in this study. These plasmids were used for biolistic transformation (Cassidy-Hanley et al., 1997), and 100 µg/mL paromomycin sulfate (Sigma-Aldrich, Cat. P8692-25G) was used to select the transformants. Deletion of the target locus from the MAC was confirmed using the primer set #3 and #4 (see below).

#	Primer name	Sequence (5'→3')
1	semi1_co-del_F	CTTTATTGTTATCATCTTATGACCGCGGATTTTACTTAATTGATTGGCAC
2	semi1_co-del_R	CTCATCAAGTTGTAATGCTAAAATGCTTGTCATAGGATTACATTCAGTAG
3	semi1_check_F	ATCCCAGAAGGATCCAAC
4	semi1_check_R	GTCAGTTTGTACGAGC

RNAi vector construction and gene knockdown

Target sequences used in hairpin RNA constructs (486 bp of the *SEMI1* ORF and 500 bp of the *ZFR3* ORF) were amplified from CU428.2 genomic DNA using PrimeSTAR Max DNA polymerase and the following primer sets: #5 and #6 for the *SEMI1* forward fragment, #7 and #8 for the *SEMI1* reverse fragment, #9 and #10 for the *ZFR3* forward fragment, and #11 and #12 for the *ZFR3* reverse fragment (see below). Amplified forward and reverse target fragments were cloned into the BamHI–BamHI and PstI–PstI sites, respectively, of pAkRNAi-NEO5 (Akematsu et al., 2018) with the NEBuilder HF DNA Assembly kit. to create the hairpin cassette. For *semi1*, the *NEO5* cassette of the backbone plasmid, which confers paromomycin resistance (Mochizuki, 2008), was replaced by a puromycin resistance marker (*PAC*) (Iwamoto et al., 2014) under the *MTT2* copper-inducible promoter (Boldrin et al., 2008, Akematsu et al., 2017) using T4 DNA ligase (New England Biolabs, Cat. M0202S). The resulting plasmids (pSEMI1i-PAC and pZFR3i-NEO5) were linearized with SacI and KpnI (New England Biolabs) before biolistic transformation. The *PAC* cassette was activated by adding 630 µM CuSO₄ to the cells, with the addition of 200 µg/mL puromycin dihydrochloride (Cayman Chemical, Ann Arbor, MI, USA, Cat. CAYM13884-500) to select transformants. RNAi was induced in cells carrying the hairpin construct by adding 0.075 µg/mL CdCl₂ during pre-conjugation starvation to promote double stranded RNA expression from the *MTT1* cadmium-inducible promoter (Shang et al., 2002).

#	Primer name	Sequence (5'→3')
5	semi1_RNAi_5F	TAAACTTAAACATCCCGGGGGATCCGCTAAACAAAAAGTGAGGGAAAGCC
6	semi1_RNAi_5R	TTGCATATCCGTTACTTACGGATCCCTTCATGAGATGACTTTTGAGAGCTG
7	semi1_RNAi_3F	TAAAAGAAGAATTCAAAGGCTGCAGTTCATGAGATGACTTTTGAGAGCTG
8	semi1_RNAi_3R	GCTGACCGATTTCAGTTCGCCTGCAGGCTAAACAAAAAGTGAGGGAAAGCC
9	zfr3_RNAi_5F	TAAACTTAAACATCCCGGGGGATCCCACTTTGAAGAGACATAATCTTCAG
10	zfr3_RNAi_5R	TTGCATATCCGTTACTTACGGATCCCTGTTAGAGTCATCATTATTAGAATATCTAG
11	zfr3_RNAi_3F	TAAAAGAAGAATTCAAAGGCTGCAGCTGTTAGAGTCATCATTATTAGAATATCTAG
12	zfr3_RNAi_3R	GCTGACCGATTTCAGTTCGCCTGCAGCACTTTGAAGAGACATAATCTTCAG

C-terminal epitope tagging

For the expression of Semi1-FZZ (composed of 3× FLAG, a TEV protease-cleavage site, and ZZ domain of protein A (Lee and Collins, 2007), Ftt18-EGFP, and Zfr3-FZZ, C-terminal tagging of endogenous proteins was done using a knock-in strategy (Kataoka et al., 2010). In short, approximately 1 kb from the 3' end of the coding sequence and 1 kb from a downstream region were amplified with PrimeSTAR Max DNA polymerase and the following primer sets: *SEMI1*, #13 and #14 for the C-terminus and #15 and #16 for the downstream region; *FTT18*, #17 and #18 for the C-terminus and #19 and #20 for the downstream region; and *ZFR3*, #21 and #22 for the C-terminus and #23 and #24 for the downstream region (see below). Amplified fragments were cloned into the pFZZ-NEO4 (GenBank: AB570112.1) or pEGFP-NEO4 (GenBank: AB570109.1) plasmid using the NEBuilder HF DNA Assembly kit or T4 DNA ligase. The resulting plasmids (pSEMI1-FZZ-NEO4, pFTT18-EGFP-NEO4, and pZFR3-FZZ-NEO4) were linearized by digestion with *SacI* and *KpnI* before biolistic transformation of *T. thermophila* cells. The *NEO4* cassette was activated by adding 1 µg/mL CdCl₂ to the cells, with 100 µg/mL paromomycin sulfate (Sigma-Aldrich) used to select the transformants.

#	Primer name	Sequence (5'→3')
13	semi1_Ctag_5F	AAAGGGAACAAAAGCTGGAGCTCGACATTC AATGGACTGTTTGGGAGA
14	semi1_Ctag_5R	TCATGATCTTTGTAATCGGATCCATAATAAAATATTAGTAAAAATAACAAAATAGCAAC
15	semi1_Ctag_3F	AGTCTCGAGGTTCAATAATGCATAGATAGTTACAACC
16	semi1_Ctag_3R	AGTCGGTACCTCCGGGTTAGATATCAACAATAGGTTAT
17	ftt18_Ctag_5F	CTAAAGGGAACAAAAGCTGGAGCTCGTAGTAAGCGGTCAACTACATTACT
18	ftt18_Ctag_5R	CTTACCCTTAGAAACCATGGATCCTTCTTATTATTCTTCAGCATCGTCT
19	ftt18_Ctag_3F	GCTTATCGATACCGTGCACCTCGAGGAGATGGTGTGAAAATCAAACAAA
20	ftt18_Ctag_3R	CTCACTATAGGGCGAATTGGGTACCGTGCTAATGAATTCGCCAAATAGC
21	zfr3_Ctag_5F	AAAGGGAACAAAAGCTGGAGCTCGCGATGAAAAATCTGAAATCAAGAA
22	zfr3_Ctag_5R	AAGTCTTACCCTTAGAAACCATGGATCCATTTTGATTTAGTTTCAATAGCTTTTG
23	zfr3_Ctag_3F	GCTTATCGATACCGTGCACCTCGAGGAGAAATAATCTTTAATGTTAACTTGAAATATCC
24	zfr3_Ctag_3R	CACTATAGGGCGAATTGGGTACCTTTGCGGAATCAGAAATTGATCTGC

N-terminal epitope tagging

The *SEMI1*, *ZFR3*, and *NUP93* ORFs were amplified from CU428.2 genomic DNA with PrimeSTAR Max DNA polymerase and the following primer sets: #25 and #26 for the *SEMI1* ORF, #27 and #28 for the *ZFR3* ORF, and #29 and #30 for *NUP93* ORF (see below). Amplified fragments were cloned into the BamHI-SpeI sites of pBNMB1-EGFP (a gift from Dr. Kazufumi Mochizuki, Institute of Human Genetics, Montpellier,

France), which contains the *MTT1* promoter, *NEO5* cassette, and the 5' and 3' portions of the *BTU1* genomic locus for homologous recombination, using the NEBuilder HF DNA Assembly kit. To transfect these plasmids into paromomycin-resistant mutant strains, we replaced the *NEO5* cassette in the plasmids with the *PAC* cassette, excised from pSEMI1i-PAC with Sall plus XmaI (New England Biolabs), using T4 DNA ligase. For Semi1 and Nup93 tagging, the *EGFP* cassette was replaced by the *mCherry* cassette, which was amplified from pmCherry-NEO4 (GenBank: AB570110.1) using PrimeSTAR Max DNA polymerase and primers #31 and #32 (see below). The resulting plasmids (pmCherry-SEMI1-PAC, pEGFP-ZFR3-NEO5, pEGFP-ZFR3-PAC, and pmCherry-NUP93-PAC) were linearized by digestion with SacI and KpnI before biolistic transformation. Protein expression was induced in cells by adding 0.075 µg/mL CdCl₂ to starved cells.

#	Primer name	Sequence (5'→3')
25	semi1_Ntag_F	GGATGAATTATATAAGGGATCCATGGATTTTACTTAATTGATTGGCAC
26	semi1_Ntag_R	CGATTCAGTTCGCTCAACTAGTATAATAAAAATATTAGTAAAAATAACAAAATAGC
27	zfr3_Ntag_F	GGATGAATTATATAAGGGATCCATGCAACACTTTGAAGAGACATAATC
28	zfr3_Ntag_R	GACCGATTCAGTTCGCTCAACTAGTATTTTGGATTTAGTTTCAATAGCTTTTG
29	Nup93_Ntag_F	GGATGAATTATATAAGGGATCCATGAGTTTTACTGTTGCTCGCGATG
30	Nup93_Ntag_R	CGATTCAGTTCGCTCAACTAGTAACCTAATCTGTAACCTAGGCATTG
31	mcherry_F	AAATAATAACTAACTTAAACATATGGTTTCAAAGGAGAAGAAGATA
32	mcherry_R	CAAGTAAATGCTCTAACATGGATCCACTAGTTTTGTAAAGTTCATCCATA

Construction of strains expressing truncated mCherry-Semi1

The *SEMI1* ORF lacking the transmembrane portion (691–711Δ) was amplified from CU428.2 genomic DNA using PrimeSTAR Max DNA polymerase and primers #33 and #34 (see below). The amplified fragment was cloned into SpeI–SpeI sites of pmCherry-SEMI1-PAC using the NEBuilder HF DNA Assembly kit. The sequence encoding the cytoplasmic portion of Semi1 (1–690) was removed from pmCherry-SEMI1-PAC by inverse PCR using PrimeSTAR Max DNA polymerase and primers #35 and #36 (see below), followed by digestion with BamHI and self-ligation with T4 DNA ligase. A free mCherry expression plasmid was also created by digesting pmCherry-SEMI1-PAC with SpeI followed by self-ligation with T4 DNA ligase. The resulting plasmids (pmCherry-691–711Δ-PAC, pmCherry-1–690Δ-PAC, and pmCherry-PAC) were linearized with SacI and KpnI before biolistic transformation. Protein expression was induced in cells by adding 0.075 µg/mL CdCl₂ during starvation.

#	Primer name	Sequence (5'→3')
33	semi1_691–711Δ_F	TATGGATGAACCTTTACAAAAGTATGGATTTTACTTAATTGATTGGCA
34	semi1_691–711Δ_R	GACCGATTCAGTTCGCTCAACTAGTATCTTTTTTTGAGTAATTGCTCTTTTC
35	semi1_1–690Δ_F	AGTCGGATCCATAGTGACAATAACTTTTTTAATTTTGTGCTATTTTG
36	semi1_1–690Δ_R	AGTCGGATCCACTAGTTTTGTAAAGTTCATCCATA

Construction of strains expressing mutated mCherry-Semi1

Inverse PCR was performed using pmCherry-SEMI1-PAC as the template and PrimeSTAR Max DNA polymerase and the following primer sets containing overlapping sequences: 109–120Δ, #37 and #38; 273–279Δ, #39 and #40; and 645–655Δ, #41 and #42 (see below). Amplified fragments were used to transform NEB 5-alpha *E. coli* cells. The resulting plasmids (pmCherry-109–120Δ-PAC, pmCherry-273–279Δ-PAC, and pmCherry-645–655Δ-PAC) were linearized by digestion with SacI and KpnI before biolistic transformation. Protein expression was induced in cells by adding 75 ng/mL CdCl₂ during starvation.

#	Primer name	Sequence (5'→3')
37	semi1_109-120Δ_F	GCTTGAAAATGATTTTATTAGCCATGAATTTTTTTG
38	semi1_109-120Δ_R	AAATCATTTTTCAAGCATTTACTATTTCATTTAAATCCT
39	semi1_273-279Δ_F	TATTTTAAGATTTTTTAAATCTTTTTTAAATGAGTTATGATAC
40	semi1_273-279Δ_R	AAAAATCTTAAATATGATTTTCTTAAACAAAACATTTTAAC
41	semi1_645-655Δ_F	AATTTTTGTGAACATCTCAGACATATGG
42	semi1_645-655Δ_R	ATGTTCAAAAAATTATTGATTGTTAGTCTTCAGG

DAPI staining

A suspension of cells was fixed by the addition of formaldehyde and Triton X-100 (final concentrations of 4% and of 0.5%, respectively). After careful mixing, cells were incubated for 30 min at room temperature and then centrifuged. The cell pellet was resuspended in 1/10 volume of 4% formaldehyde + 3.4% sucrose. A total of 80 µL of this mixture was spread onto a clean slide and air-dried. For chromosome staining, slides were incubated for 10 min in phosphate buffered saline (PBS) and mounted under a coverslip in Vectashield anti-fading agent (Vector Laboratories, Burlingame, CA, USA, H-1000) containing 50 µg/mL DAPI.

Immunocytology

For immunostaining of Rad51, slides prepared by the same method as for DAPI staining were incubated for 10 min in PBS containing 0.05% Triton X-100 and then in PBS. An anti-Rad51 antibody (1:100 dilution; mouse monoclonal, Lab Vision/NeoMarkers, Fremont, CA, USA, RRID: AB_144075) was then applied, and incubated under a coverslip overnight at 4°C. The slides were then rinsed with PBS for 10 min. FITC-labeled goat anti-mouse antibody (1:500 dilution; Merck Millipore, Burlington, MA, USA, RRID: AB_92634) was applied and incubated under a coverslip at room temperature for 1 h in the dark. Finally, the slides were incubated twice for 10 min in PBS and mounted under a coverslip in Vectashield anti-fading agent containing 50 µg/mL DAPI. For γH2AX and H3K56ac immunostaining, cells were fixed in methanol at -20°C for 1 h. After removal of methanol by centrifugation (3000 × g, 1 min), the cell pellet was postfixed in 1% paraformaldehyde dissolved in PBS at 4°C for 1 h. After the removal of paraformaldehyde by centrifugation, the pellet was resuspended in PBS and incubated for 1 h at room temperature with primary antibodies: anti-γH2AX (1:500 dilution; mouse monoclonal; BioLegend, San Diego, CA, USA, RRID: AB_315794) and anti-H3K56ac (1:500 dilution; rabbit polyclonal; Active Motif, Carlsbad, CA, USA, RRID: AB_2661786) antibodies. After washing with PBS, cells were incubated with FITC-labeled goat anti-mouse (1:500 dilution) and Rhodamine-labeled goat anti-rabbit (1:2000 dilution; Merck Millipore, RRID: AB_90296) secondary antibodies for 1 h at room temperature in the dark. After washing with PBS, cells were resuspended in Vectashield anti-fading agent containing 50 µg/mL DAPI, dropped onto a slide and mounted under a coverslip.

Fluorescence microscopy of living cells

Living cells in 10 mM Tris-HCl (pH 7.4) were incubated with Hoechst33342 (50 ng/mL; Invitrogen, Carlsbad, CA, USA, Cat. H3570) at 30°C for 30 min. After incubation, the cells were concentrated by centrifugation, resuspended in 3% polyethylene oxide to increase the viscosity of the medium, and 1 µL of the cell suspension was placed into a Commodore Compressor device (Yan et al., 2014) to immobilize the cells for microscopic inspection.

Western blotting

Cells were fixed with 10% (w/v) trichloroacetic acid (TCA) to prevent proteolysis and incubated on ice for 30 min. After removal of TCA by centrifugation at 9000 × g for 1 min, cell pellets were lysed in polyacrylamide gel electrophoresis (PAGE) sample buffer (6% SDS, 6% 2-mercaptoethanol, 5% glycerol 36% urea, and 360 mM Tris- HCl, pH6.8) and boiled at 98°C for 3 min; 10 µg total protein was loaded into each lane of Mini-PROTEAN TGX Precast Gel (4–15%; Bio-Rad, Hercules, CA, USA, Cat. 4561083),

separated by SDS-PAGE, and transferred onto a polyvinylidene fluoride membrane (Bio-Rad). Membranes were washed in PBS-T (0.05% Tween 20 in PBS), blocked in 5% dry skimmed milk in PBS-T for 30 min, and incubated for 1 h at room temperature with anti-flag (1:2000; mouse monoclonal; Sigma-Aldrich, RRID: AB_259529), anti-RFP (1:2000; mouse monoclonal; ChromoTek, Planegg-Martinsried, Germany, RRID: AB_2631395), or anti-tubulin α (1:10,000; mouse monoclonal; Lab Vision/NeoMarkers, RRID: AB_144075) antibody. After washing in PBS-T, membranes were incubated in PBS-T containing 5% dry skimmed milk and horseradish peroxidase-conjugated goat anti-mouse IgG antibody (1:5000; Bio-Rad, RRID: AB_808614) for 1 h at room temperature. Membranes were washed with PBS-T and developed using Clarity Western ECL (Bio-Rad, Cat. 1705060). Restore Western Blot Stripping Buffer (Thermo Fisher Scientific, Waltham, MA, USA, 21059) was used to reprobe membranes.

Co-immunoprecipitation and mass spectrometry

For co-immunoprecipitation, mCherry-Semi1-expressing cells were pretreated with 0.5 mM phenylmethylsulfonyl fluoride (PMSF; Cell Signaling Technology, Danvers, MA, USA, Cat. 8553S) for 30 min at 30°C (Iwamoto et al., 2017) and then collected by centrifugation at $700 \times g$ for 3 min. The cells were resuspended at 1.5×10^7 cells/mL in homogenization buffer composed of 150 mM NaCl, 1% Triton X-100, 2 mM PMSF, and Complete Protease Inhibitor Cocktail (Sigma-Aldrich, P8215-1ML), and homogenized by gentle pipetting on ice for 30 min. The lysate obtained after clarification at $10,000 \times g$ for 15 min was incubated with 25 μ L RFP-Trap magnetic agarose beads (ChromoTek, Cat. rtma-20; pretreated with 5 mM Sulfo-NHS-Acetate [Thermo Fisher Scientific, Cat. 26777]) at 4°C for 1 h. After three washes with 150 mM NaCl, the beads bearing immunoprecipitated proteins were submitted to the Mass Spectrometry Facility of the Max F. Perutz Laboratories (Vienna, Austria). To identify significant interaction partners from the affinity purification data, MS data were analyzed using SAINTexpress (Teo et al., 2014). The average SAINT scores were calculated for two experimental samples for each bait analyzed and a p value of <0.05 was considered to indicate a biologically significant interaction.

EdU incorporation assay

WT CU428.2 or *semi1* Δ mating type VI cells were incubated overnight in 10 mM Tris-HCl (pH 7.4) containing 50 μ M 5-ethynyl-2'-deoxyuridine (EdU, Thermo Fisher Scientific, C10337). The cells were then washed with fresh 10 mM Tris-HCl (pH 7.4) and mixed with B2086 or *semi1* Δ mating type IV cells. After 5 h and 10 h, 30 μ L cell suspension was put onto poly-L-lysine-coated slides and air-dried. The slides were then soaked in fixation solution (50 mM glycine dissolved in ethanol, pH 2.0) for 20 min at -20°C and then washed in PBS for 10 min at room temperature. Click-iT EdU Alexa Fluor reaction cocktail (Thermo Fisher Scientific, C10337) was applied and incubated under a coverslip for 30 min at room temperature. The slides were washed twice for 10 min in PBS and mounted under a coverslip in Vectashield anti-fading agent containing 50 μ g/mL DAPI.

Supplemental References

- AKEMATSU, T., FINDLAY, A., FUKUDA, Y., PEARLMAN, R. E., LOIDL, J., ORIAS, E. & HAMILTON, E. P. 2018. Resistance to 6-Methylpurine is Conferred by Defective Adenine Phosphoribosyltransferase in Tetrahymena. *Genes (Basel)*, 9, 179.
- AKEMATSU, T., FUKUDA, Y., GARG, J., FILLINGHAM, J. S., PEARLMAN, R. E. & LOIDL, J. 2017. Post-meiotic DNA double-strand breaks occur in Tetrahymena, and require Topoisomerase II and Spo11. *Elife*, 6.
- BOLDRIN, F., SANTOVITO, G., FORMIGARI, A., BISHARYAN, Y., CASSIDY-HANLEY, D., CLARK, T. G. & PICCINNI, E. 2008. MTT2, a copper-inducible metallothionein gene from Tetrahymena thermophila. *Comp Biochem Physiol C Toxicol Pharmacol*, 147, 232-40.
- CASSIDY-HANLEY, D., BOWEN, J., LEE, J. H., COLE, E., VERPLANK, L. A., GAERTIG, J., GOROVSKY, M. A. & BRUNS, P. J. 1997. Germline and Somatic Transformation of Mating Tetrahymena thermophila by Particle Bombardment. *Genetics*, 146, 135-147.
- HAYASHI, A. & MOCHIZUKI, K. 2015. Targeted Gene Disruption by Ectopic Induction of DNA Elimination in Tetrahymena. *Genetics*, 201, 55-64.
- IWAMOTO, M., MORI, C., HIRAOKA, Y. & HARAGUCHI, T. 2014. Puromycin resistance gene as an effective selection marker for ciliate Tetrahymena. *Gene*, 534, 249-55.
- IWAMOTO, M., MORI, C., KOJIDANI, T., BUNAI, F., HORI, T., FUKAGAWA, T., HIRAOKA, Y. & HARAGUCHI, T. 2009. Two distinct repeat sequences of Nup98 nucleoporins characterize dual nuclei in the binucleated ciliate tetrahymena. *Curr Biol*, 19, 843-7.
- IWAMOTO, M., OSAKADA, H., MORI, C., FUKUDA, Y., NAGAO, K., OBUSE, C., HIRAOKA, Y. & HARAGUCHI, T. 2017. Compositionally distinct nuclear pore complexes of functionally distinct dimorphic nuclei in the ciliate Tetrahymena. *J Cell Sci*, 130, 1822-1834.
- KATAOKA, K., SCHOEBERL, U. E. & MOCHIZUKI, K. 2010. Modules for C-terminal epitope tagging of Tetrahymena genes. *J Microbiol Methods*, 82, 342-6.
- LEE, S. R. & COLLINS, K. 2007. Physical and functional coupling of RNA-dependent RNA polymerase and Dicer in the biogenesis of endogenous siRNAs. *Nat Struct Mol Biol*, 14, 604-10.
- MOCHIZUKI, K. 2008. High efficiency transformation of Tetrahymena using a codon-optimized neomycin resistance gene. *Gene*, 425, 79-83.
- MOCHIZUKI, K., NOVATSKOVA, M. & LOIDL, J. 2008. DNA double-strand breaks, but not crossovers, are required for the reorganization of meiotic nuclei in Tetrahymena. *J Cell Sci*, 121, 2148-58.
- SHANG, Y., SONG, X., BOWEN, J., CORSTANJE, R., GAO, Y., GAERTIG, J. & GOROVSKY, M. A. 2002. A robust inducible-repressible promoter greatly facilitates gene knockouts, conditional expression, and overexpression of homologous and heterologous genes in Tetrahymena thermophila. *Proc Natl Acad Sci U S A*, 99, 3734-9.
- TEO, G., LIU, G., ZHANG, J., NESVIZHSHKII, A. I., GINGRAS, A. C. & CHOI, H. 2014. SAINTexpress: improvements and additional features in Significance Analysis of INteractome software. *J Proteomics*, 100, 37-43.
- YAN, Y., JIANG, L., AUFDERHEIDE, K. J., WRIGHT, G. A., TEREKHOV, A., COSTA, L., QIN, K., MCCLEERY, W. T., FELLENSTEIN, J. J., USTIONE, A., ROBERTSON, J. B., JOHNSON, C. H., PISTON, D. W., HUTSON, M. S., WIKSWO, J. P., HOFMEISTER, W. & JANETOPOULOS, C. 2014. A microfluidic-enabled mechanical microcompressor for the immobilization of live single- and multi-cellular specimens. *Microsc Microanal*, 20, 141-51.